SANDIA REPORT

SAND 2010-0698
Unlimited Release
February 2010

New Mexico Cloud Super-Cooled Liquid Water Survey Final Report 2009

John K. Roskovensky (5713)
Mark Ivey (6338)
Nick Beavis (6338)

Sandia National Laboratories
P.O. Box 5800
Albuquerque, New Mexico 87185

Prepared by
Sandia National Laboratories
Albuquerque, New Mexico 87185 and Livermore, California 94550

Sandia is a multiprogram laboratory operated by Sandia Corporation,
a Lockheed Martin Company, for the United States Department of Energy's
National Nuclear Security Administration under Contract DE-AC04-94AL85000.

Issued by Sandia National Laboratories, operated for the United States Department of Energy by Sandia Corporation.

Available to DOE and DOE contractors from
U.S. Department of Energy
Office of Scientific and Technical Information
P.O. Box 62
Oak Ridge, TN 37831

Telephone: (865) 576-8401
Facsimile: (865) 576-5728
E-Mail: reports@adonis.osti.gov
Online ordering: http://www.osti.gov/bridge

Available to the public from
U.S. Department of Commerce
National Technical Information Service
5285 Port Royal Rd.
Springfield, VA 22161

Telephone: (800) 553-6847
Facsimile: (703) 605-6900
E-Mail: orders@ntis.fedworld.gov
Online order: http://www.ntis.gov/help/ordermethods.asp?loc=7-4-0#online

SAND 2010-0698
Unlimited Release
February 2010

New Mexico Cloud Super Cool Liquid Water Survey Final Report 2009

John K. Roskovensky (5713)
Mark Ivey (6338)
Nick Beavis (6338)
Sandia National Laboratories
P.O. Box 5800
Albuquerque, New Mexico 87185 MS0406

Abstract

Los Alamos and Sandia National Laboratories are partners in an effort to survey the super-cooled liquid water in clouds over the state of New Mexico in a project sponsored by the New Mexico Small Business Assistance Program. This report summarizes the scientific work performed at Sandia National Laboratories during the 2009. In this second year of the project a practical methodology for estimating cloud super-cooled liquid water was created. This was accomplished through the analysis of certain MODIS sensor satellite derived cloud products and vetted parameterizations techniques. A software code was developed to analyze multiple cases automatically. The eighty-one storm events identified in the previous year effort from 2006-2007 were again the focus. Six derived MODIS products were obtained first through careful MODIS image evaluation. Both cloud and clear-sky properties from this dataset were determined over New Mexico. Sensitivity studies were performed that identified the parameters which most influenced the estimation of cloud super-cooled liquid water. Limited validation was undertaken to ensure the soundness of the cloud super-cooled estimates. Finally, a path forward was formulized to insure the successful completion of the initial scientific goals which include analyzing different of annual datasets, validation of the developed algorithm, and the creation of a user-friendly and interactive tool for estimating cloud super-cooled liquid water.

ACKNOWLEDGMENTS

This work was funded through the New Mexico Small Business Assistance Program. The NMSBA Programs at Sandia and Los Alamos National Laboratories were created in response to New Mexico's Laboratory Partnership with Small Business Tax Credit Act. The authors would like to thank Bill Porch at LANL for his excellent leadership as Principal Investigator and project partner; Lisa Henne, for her superb guidance; and Sigmund Silber for his genuine support and for the valuable insight and direction that he has lent to this work.

CONTENTS

FIGURES

TABLES

ACRONYMS

AOD	Aerosol Optical Depth
AOI	Area-Of-Interest
ARM	Atmospheric Radiation Measurement
CCN	Cloud Condensation Nuclei
COD	Cloud Optical Depth
CSEA	Cloud Super-cooled liquid water Estimation Algorithm
CTP	Cloud Top Pressure
CTT	Cloud Top Temperature
ENVI	Environment for Visualizing Images
FOV	Field-Of-View
GCM	General Circulation Models
GMT	Greenwich Mean Time
GOES	Geostationary Operational Environmental Satellites
GUI	Graphical User Interface
I/O	Input ant Output
IDL	Interactive Data Language
IR	Infrared
LOS	Line-Of-Sight
LWIR	Long-Wave Infrared
MALR	Moist Adiabatic Lapse Rate
MODIS	Moderate Resolution Imaging Spectroradiometer
NASA	National Aeronautics and Space Administration
NMSBA	New Mexico Small Business Assistance Program
POLDER	Polarization and Directionality of the Earth's Reflectances
RGB	Red, Green, and Blue tri-color image
ROI	Region-Of-Interest
RSI	Research Systems, Inc
SLW	Super-cooled Liquid Water
SNL	Sandia National Laboratories

1. INTRODUCTION

This report summarizes the work performed at Sandia National Laboratories during the second year of the New Mexico Small Business Assistance (NMSBA) Program sponsored project to survey the cloud Super-cooled Liquid Water (SLW) over the state. It continues on the first year's effort that was summarized in a SAND report (Roskovensky et al., 2009). Procedures and datasets previously defined in the initial project year were further developed in-line with the original project goals. Figure 1 provides a list of the major accomplishments established annually for this project. Successive yearly goals and accomplishments are built on those of the previous year and follow a logic order needed to realize the final year's deliverables. At the end of the first year, relevant satellite and ground-based datasets were identified that could be relied upon to produce viable estimates of cloud SLW. Using images from a Geostationary Operational Environmental Satellite (GOES) dataset, specific storm event cases (daily events) were identified as having sufficient cloud cover to warrant further investigation. A software program was created to handle and analyze satellite and ground data from multiple events. Finally, a crude proof-of-concept cloud SLW estimation algorithm was made to output preliminary results. The effort this year utilized the previous accomplishments to develop a more realistic cloud SLW estimation algorithm that has been initially validated. Vast quantities of satellite data from the Moderate Resolution Imaging Spectroradiometer (MODIS) sensor as well as surface data corresponding to the dates and times identified by the GOES study were selected and obtained. Handling routines for this data with respect to accessing, reading, unpacking, and scaling were devised. Computer code was then developed to analyze cloud and clear-sky properties for the selected cases in a single algorithm run. Validation of the algorithm and its results has also begun. A path forward for the third and final year of the project has been constructed. Work from the second year will be leveraged in many ways. The software encapsulating the cloud SLW estimation algorithm is mature enough to be used to study datasets from different years pertaining to extreme dry and wet conditions. Annual data from these particular periods are already beginning to be identified and obtained. A concept for a user friendly tool to control and interact with the cloud SLW estimation algorithm has been developed with input from our private-sector partner in the project. Finally, algorithm validation protocols have been installed within the software.

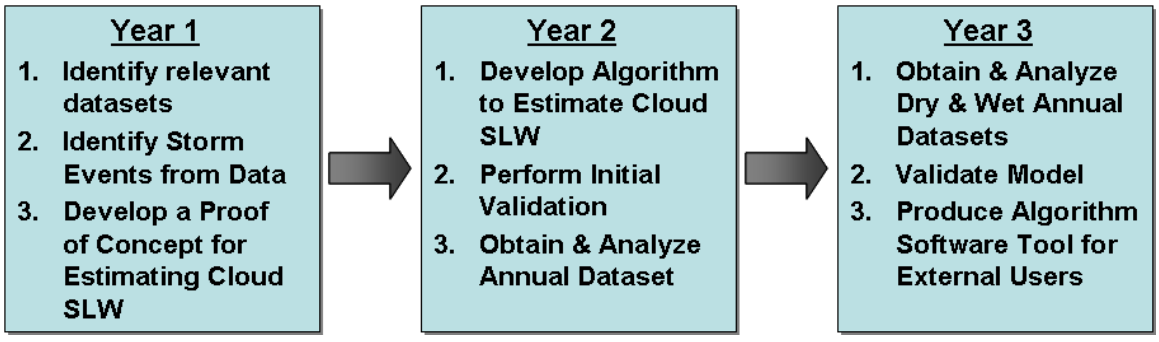

Figure 1. Cloud SLW algorithm development annual accomplishment lists.

A great deal of progress in estimating cloud SLW over New Mexico has been made. Preliminary cloud SLW volume calculations of the initial year have been transformed into a mature and robust algorithm. Corresponding software code has been developed to produce spatial and mean results of various cloud and clear-sky properties over the state of New Mexico. In order to do this, appropriate datasets have been collected. This somewhat tedious task of identifying the specific data that spatially corresponded to the state of New Mexico followed by ordering and downloading the resulting numerous datasets was completed. At the same time, the software program was developed to process and evaluate multiple datasets. Switches were put in the code to control input of data as well as certain computational procedures. Effort was spent on geo-locating and producing data templates at various pixel resolutions. This was needed because MODIS derived products are produced at different horizontal resolutions. Due to the need for derived cloud top temperature, the cloud SLW estimate was constructed at the same 5 km x 5 km spatial resolution. A new, more realistic estimation procedure for cloud SLW content was a major focus. Using MODIS derived cloud top temperature and cloud optical depth, the cloud vertical thickness was estimated. Vertical cloud temperatures were then extrapolated by employing a standard moist adiabatic lapse rate downward through the vertical length from the cloud top where the temperature was derived. Another parameterization was employed to determine the fractional density of super-cooled liquid water to that of total cloud particle density. This liquid water fraction was determined for each unit of temperature for cloud temperatures below 0º C. vertical column SLW totals were calculated using the MODIS derive cloud water path and the approximate SLW fraction. This was turned into a cloud SLW mass value per pixel so that total cloud SLW amounts over user defined areas-of-interest (AOI) could be easily derived.

One of the crucial approximations in which estimated cloud SLW is very sensitive occurs in the cloud thickness estimation parameterization. Since the cloud temperature range is directly proportional to the vertical cloud thickness, cloud SLW estimates vary a great deal depending on the range of temperatures calculated to be below the freezing mark. Initial validation of the cloud thickness parameterization has begun through the comparison of algorithm results with those measured by the CloudSat satellite radar sensor. The CloudSat instrument orbits directly behind the MODIS sensor onboard the Aqua platform by roughly 1-minute, therefore, providing nearly simultaneous comparisons. Unlike the passive measurements of MODIS, radar can penetrate through cloud to define the cloud top, base, and, thus, thickness. Validation of other algorithm estimated properties including cloud optical depth and cloud liquid water path are also possible using CloudSat derived products. Validation of cloud SLW is more difficult since accurate quantification generally requires *in-situ* measurements. Preliminary validation was done earlier in the project using radiometer data from the Atmospheric Radiation Measurement (ARM) site in Oklahoma.

This paper is organized in the following manner. The process used to select and obtain the large dataset as well as a description of the data is presented first. Section 3 details the individual steps followed by the cloud SLW estimations algorithm. The algorithm

results and specific analysis are presented and discussed in section 4. Validation procedures and results are outlined in section 5. The paper ends with a summary and discussion about future work.

2. DATA ACQUISITION

This section describes the data obtained and utilized during the second year of this project for estimating and validating the cloud super-cooled liquid water content as well as characterizing the ambient environmental conditions present. The datasets that are used to derive spatial cloud SLW content are many of the MODIS derived cloud products. Other non-cloud derived products are also obtained for clear-sky property assessment. Space-borne radar data from the CloudSat instrument is used to validate some of the derived MODIS products and newly estimated properties. A description of the satellite products obtained for this project is given in the first part of this section. The second sub-section discusses the surface data that were obtained and used in part to characterize the ambient environment conditions.

2.1 Satellite Data

The satellite data utilized in the effort this year were primarily from the MODIS sensor. Analysis of GOES imagery identified the daily events that had sufficient cloud cover to be of interest very near the overpass time of the MODIS sensor that is onboard the Terra satellite. MODIS data, along with CloudSat radar data products, are described in detail in separate sub-sections.

2.1.1 MODIS Data

MODIS data products were obtained for eighty-one of the cases that were identified as having at least 30% detected cloud cover in either the northern or southern region of New Mexico by the GOES images taken at 1745 GMT between 10 March 2006 and 10 May 2007. A full list of the dates and times where MODIS data were obtained is given in Table 11 in the Appendix along with the corresponding Julian day, since that is the formatted date used in the MODIS products. Data collected from the MODIS sensor onboard the Terra satellite corresponded fairly well in time with the GOES imagery previously examined. The Terra satellite is in a near sun-synchronous orbit with a local equator overpass time of about 10:30 am. At New Mexico's longitude this equates to roughly 1730 GMT which was very near the 1745 GMT GOES collection. The actual MODIS collection times seen in Table 11 vary by 95 minutes (1705 to 1840) due to data collected from successive orbits which are about 90 minutes apart. This daily variation makes the acquisition of the MODIS data somewhat tedious because imagery must be examined to ensure appropriate area coverage before data are ordered. MODIS data are packaged as granules in five minute collection periods. At the 1 km nadir pixel resolution, each granule possesses either 2030 or 2040 total scanlines each containing 1354 pixels. The spatial coverage area of each granule is about 2000 km x 2000 km. On certain days in the event dataset, the state of New Mexico was not fully contained in a single MODIS granule. In these instances, the granule that contained most of the state was acquired resulting in only partial coverage of the state.

Table 1 lists the actual MODIS derived products that were obtained for each daily event. Given in the table are the filenames followed by the dataset of interest contained in each file. These files can be obtained via the ordering protocol from the MODIS atmospheric data archive located at: http://ladsweb.nascom.nasa.gov/index.html.

Table 1. List of the MODIS datasets examined.

Filename	Dataset	Resolution	Fill Value	Scale Factor	Offset
MOD03	Latitude	1 km	-999.0	1.0	0.0
	Longitude	1 km	-999.0	1.0	0.0
MOD04	Optical Depth land and Ocean	10 km	-9999	0.001	0.0
	Angstrom Exponent land	10 km	-9999	0.001	0.0
MOD05	Water Vapor Near Infrared	1 km	-9999	0.001	0.0
	Water vapor Infrared	5 km	-9999	0.001	0.0
MOD06	Cloud_Top_Pressure	5 km	-32768	0.1	0.0
	Cloud_Top_Temperature	5 km	-32768	0.01	-15000
	Cloud_Effective_Emissivity	5 km	127	0.01	0.0
	Cloud_Phase_Infrared	5 km	127	1.0	0.0
	Cloud_Effective_Radius	1 km	-9999	0.01	0.0
	Cloud_Optical_Thickness	1 km	-9999	0.01	0.0
	Cloud_Water_Path	1 km	-9999	1.0	0.0
	Cloud_Water_Path_Uncertainty	1 km	-9999	0.01	0.0
	Cloud_Multi_Layer_Flag	1 km	0	1.0	0.0
	Cirrus_Reflectance_Flag	1 km	-99	1.0	0.0
MOD07	Surface temperature	5 km	-32768	0.01	-15000
	Surface Elevation	5 km	-32768	1.0	0.0
	Retrieved_Temperature_Profile	5 km	-32768	0.01	-15000
	Retrieved_Moisture_Profile	5 km	-32768	0.01	-15000
	Retrieved_Height_Profile	5 km	-32768	1.0	-32500
	Lifted_Index	5 km	-32768	0.01	0.0
MOD35	Cloud Mask	1 km	0	1.0	0.0

The six MODIS files contain derived datasets with the following focuses:

- MOD03: Geo-location information.
- MOD04: Aerosol products.
- MOD05: Precipitable Water product.
- MOD06: Cloud Products.
- MOD07: Atmosphere products.
- MOD35: Cloud Mask product.

Data files from the MODIS sensor onboard the Terra satellite are named, as shown in the table, with the MOD prefix. The names of the specific datasets contained in each file are listed after the filename in Table 1. Four dataset attributes are also given in the table: horizontal resolution, fill value, scale factor, and offset. The horizontal resolution is the

approximate product spatial pixel size. The resolution is dictated by the required MODIS band Signal-to-Noise Ratio (SNR) needed for property retrieval. The fill value is used when a derived data value could not be determined. The scale factor and offset are used as a multiplier and an additive value, respectively, that converts the stored data value into a scientific quantity. For more information about product descriptions and retrieval algorithms please consult the specific technical documents under Level 1 ATBDs (MOD03) and Atmosphere ATBDs which can be found and downloaded at: http://modis.gsfc.nasa.gov/data/atbd/index.php.

2.1.2 CloudSat Data

Onboard the CloudSat satellite is the cloud profiling radar which operates at 94 GHz (recognized as the standard cloud radar sensing frequency). At this wavelength, energy penetrates through cloud fairly well to produce accurate backscatter profiles which can be used to retrieve cloud properties. The radar is pointed just slightly off-nadir to reduce the effect of surface reflectance. Its resolution is about 500 m in the vertical, 1.4 km across-track, and 1.7 km along-track. As a result, it produces data that are well suited for comparison, in terms of resolution, to MODIS data. CloudSat data can be obtained at: http://www.cloudsat.cira.colostate.edu/. Derived data product descriptions are presented at: http://cloudsat.atmos.colostate.edu/data. The CloudSat data files and their derived products that were obtained in order to validate some of the properties determined from MODIS data are listed in Table 2. The last column gives the dimensions of each dataset. If a single data value is produced for each horizontal column, the * appears which signifies the number of along track pixels. The extra dimension is given if data is produced in the vertical direction.

Table 2. List of the CloudSat datasets examined.

Filename	Dataset	Dimensions
2B- GEOPROF	Latitude	*
	Longitude	*
	Height	* x 125
	Cloud Mask	* x 125
2B-TAU	Vertical Optical Depth	* x 125
	Column Optical Depth	*
2B-CWC-RVOD	Liquid Water Content	*
	Ice Water Content	*

* denotes the 1-dimension along-track pixel vector.

2.2 Surface Data

Data measurements from 16 surface data sites across the state of New Mexico were obtained in order to characterize the environmental conditions of the identified events. A list of the ground sites along with their geographic locations is given in

.

Table 3. New Mexico surface data sites utilized for precipitation measurements.

Sites	Abbreviation	Latitude	Longitude	Elevation (m)
Albuquerque Int. Sunport	ABQ	35.042	-106.615	1630.98
Chama METAR	CHM	36.900	-106.583	2393.00
Clayton LRC	CLY	36.468	-103.088	1459.00
Clovis Municipal Airport	CLO	34.433	-103.083	1285.04
Deming METAR	DEM	32.267	-107.717	1311.00
Farmington ASC	FAR	36.683	-108.310	1720.00
Frisco Divide	FRI	33.733	-108.933	2332.00
Gallup Municipal Airport	GAL	35.511	-108.789	1972.97
Hobbs/Lea County Airport	HOB	32.683	-103.217	1114.96
Jemez RAWS	JEM	35.841	-106.619	2438.10
Las Cruces International Airport	CRU	32.289	-106.922	1357.88
Las Vegas Municipal Airport	LVG	35.654	-105.143	2096.11
Red River Pass #2	RRV	36.683	-105.333	2881.00
Roswell Airport	ROS	33.300	-104.500	1112.00
Sierra Blanca	SBC	33.400	-105.783	3146.00
Socorro RAWS	SOC	34.106	-107.316	2011.38
Taos Regional Airport	TOA	36.450	-105.670	2161.03

Figure 2 shows the approximate locations of the surface data sites as listed in Table 3. Text reports of both daily and hourly temperature, humidity, wind speed, wind direction, and precipitation rates and accumulation values for each site can be ordered from the New Mexico State University website: http://weather.nmsu.edu/data/data.htm. It was found that precipitation totals from the Frisco ground site were often erroneously high. As a result, data from this site was ignored during the analysis. Only precipitation accumulation results were input into the algorithm thus far because of the very tedious task of manually constructing new ASCII input files.

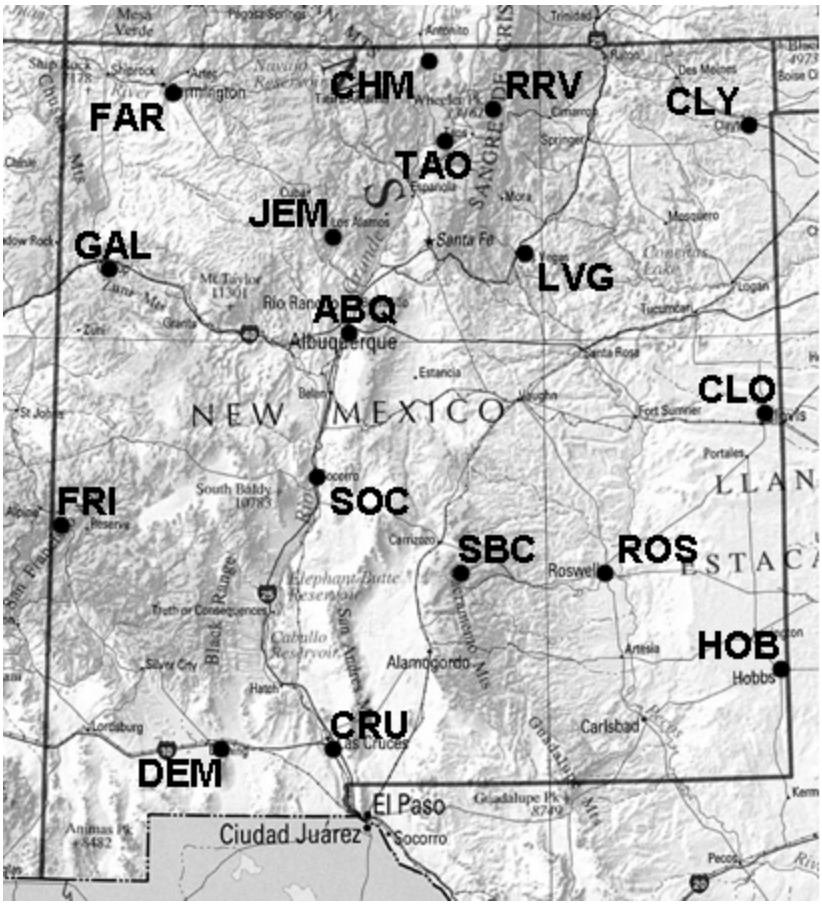

Figure 2. Locations of the New Mexican surface data sites.

3. ALGORITHM DESCRIPTION

This section describes the algorithm developed to estimate cloud super-cooled liquid water (SLW) from MODIS satellite data. The algorithm is written in Interactive Data Language (IDL), originally created by Research Systems, Inc. (RSI). IDL is a commercial software package that is maintained by a branch of ITT Industries, Inc. It requires certain manually arranged data and some initial preparation based on desired functionality. Once this is established the software is run without any interaction. It is designed to run in batch mode, meaning that it can handle multiple events. More detailed information on the processes, functionality, and scientific aspects of the algorithm and code is presented in the following subsections.

3.1 Overview

A brief overview of the Cloud Super-cooled liquid water Estimation Algorithm (CSEA) is presented here. Figure 3 displays the general flow of the algorithm by highlighting the important processes. Before running the program the input data must be arranged correctly and several control switches must be set to an *on* or *off* position. Once this is done, the code must be compiled by the IDL commercial software package. Both Windows and Unix version exist. If the compiler finds no errors, the program can be run, again by the IDL commercial package. The code is fully automated and requires no manual input as it runs. There are certain errors that will stop the code. These usually stem from incorrect data arrangement and/or program control settings or bad data. The first step the algorithm performs is the reading of the input filenames from ASCII format lists. Up to seven file lists (a directory list plus six separate MODIS file lists) must be constructed and read. These lists should contain the same number of entries corresponding to the specific events. The directory list sets the number of events, and if any subsequent list does not have the exact same number of listed filenames, a print message is sent and the program is terminated. This saves the program from producing incorrect results in later steps. If ground data exists and the ground switch is set, the program will read all of the data form all sites for all events at one time. Once the number of events is determined by the program, it starts a loop which begins before the *Read MODIS Data* step in Figure 3 and last until just before the *End* step. Each event is processed completely and successively in order. If an error occurs in the n^{th} event, data output for the previous n – 1 events will exist. For each event, reading in the MODIS data is the first function performed. Incorrect data dimension errors will occur at this point. This step is followed by the construction of an Area-of-Interest (AOI) mask based on the MOD03 file datasets. An AOI mask is made for each important resolution: *1 km, 5 km, and 10 km*. Crucial fine-resolution datasets are then aggregated to appropriate poorer-resolution based on need for products at particular scales so that direct comparison of data can be easily made in later steps.

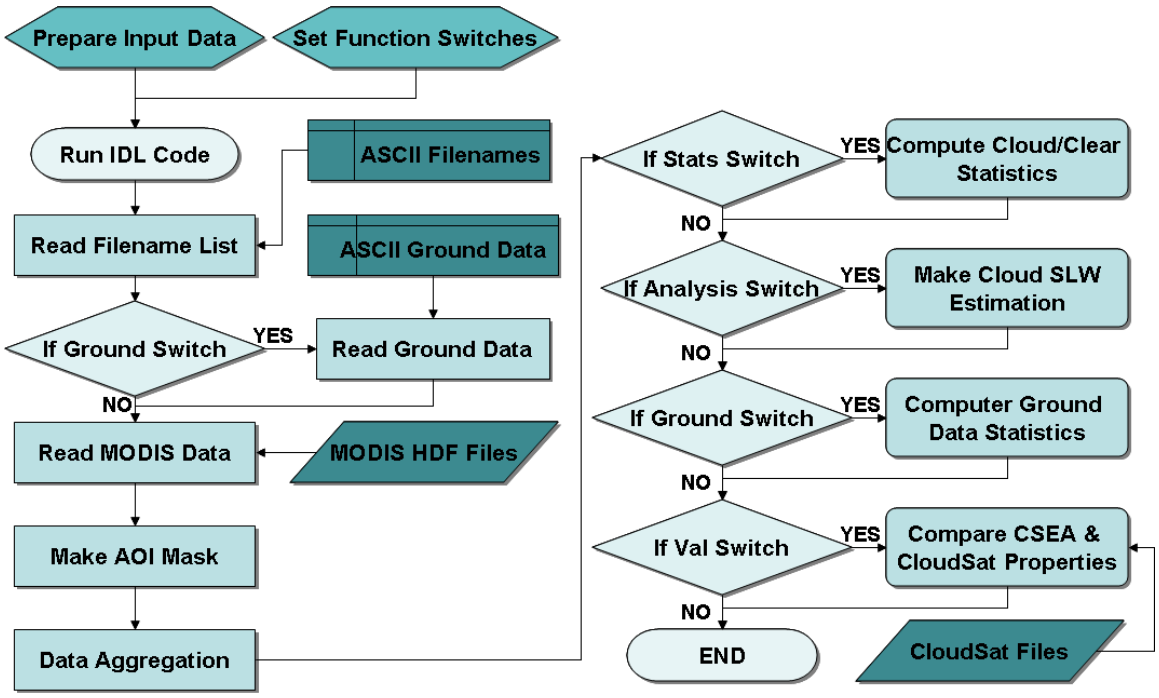

Figure 3. Cloud SLW Estimation Algorithm (CSEA) Flow Chart.

The rest of the program is designed to calculate statistical and comparison results. These processes are controlled by switches that the user has manually set before the program was run. These switches simply control whether or not each process is performed. There are four important processes that are controlled in this way and their serial implementation is depicted on the right side of the flow chart shown in Figure 3. The first process computes bulk cloud and clear-sky properties in the AOI. The second process performs the cloud SLW estimation. The third process analyzes any input ground data that was previously read. The fourth process analyzes CloudSat data products and compares them to the MODIS/CSEA properties for validation. Eventually, CloudSat data could be used to adjust certain cloud properties used in the CSEA code.

Output occurs automatically throughout program as products are made and statistics produced which is not reflected in flow chart. The algorithm runtime is roughly about 20 seconds per event when the full functionality is performed. The runtime for the 81 selected cases previously discussed took about 28 minutes to finish on a standard PC although this time will vary a great deal based on the machine used. The following subsections provide greater detail of the specific processes and methodologies discussed and alluded to thus far.

3.2 Input and Output

Specific arrangement of the input data must be made by the user so the program operates correctly. Also, the program produces a great deal of output automatically. The details on these two aspects are discussed separately below.

3.2.1 Input

Input to the CSEA code must be placed at a certain location or directory path. Any ground data file should be put at that location. The MODIS data files need to be saved in specific directories at that same location. A unique directory should be made for each event and all the MODIS HDF files for that event should be stored inside. The directories may have any name, but a logical naming convention uses the MODIS date format YYYYJJJ where Y stands for the 4-digit year value, and, J, the three-digit Julian day. Figure 4 shows the screen capture of the contents of a MODIS data directory for the MODIS event date of 11 March 2006 (2006070). The first six files are the MODIS HDF input files. The other files are all CSEA code output which will be discussed in the next section.

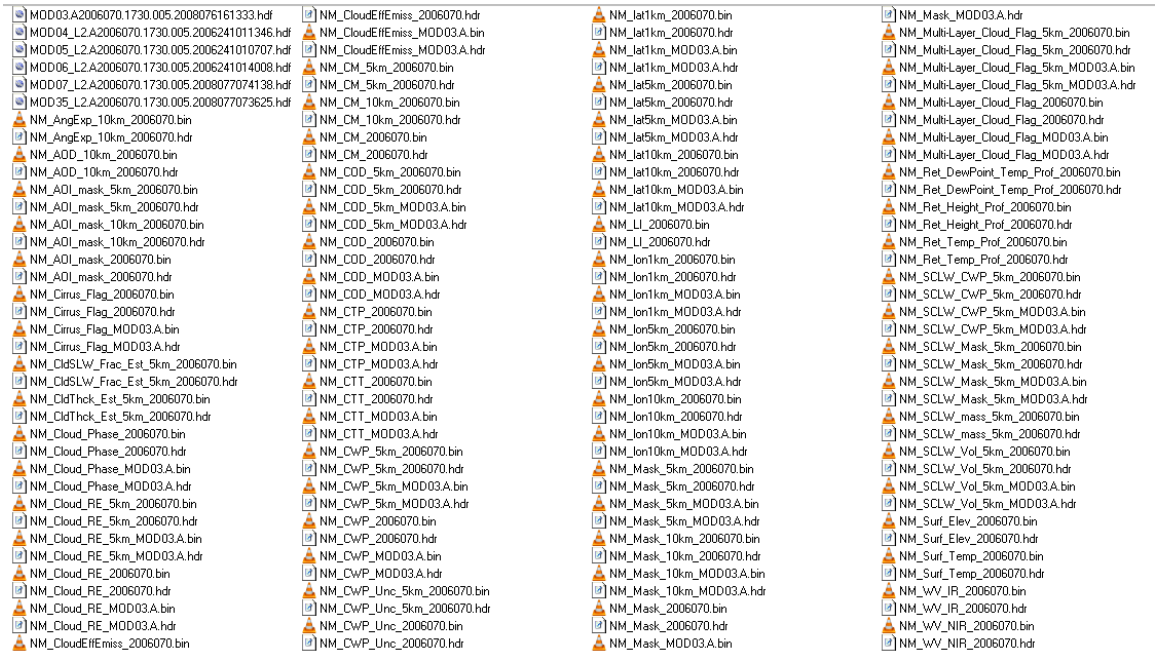

Figure 4. Screen capture of the contents of a MODIS data directory.

Surface data files are presently constructed manually and located at the specified data path. They are ASCII (text) file constructed by text editors such as notepad or wordpad or by saving an excel spreadsheet as a text file. These files must adhere to a specified format. Data should be separated by a space. The number of lines in the file is dictated by the number of ground sites. The first two columns must contain the latitude and longitude of the ground site, respectively. Each successive column must contain the data value for ordered events for each ground site. As a result of this intensive manual effort to create these files, the only ground data input file made thus far contains precipitation accumulation data from the events in 2007. In the future, it may be possible to write code to retrieve ground data automatically from the text reports obtained from the NMSU site. Unfortunately, the NMSU format is likely to be unique and different than ground data from other regions. Re-coding the program to read ground data from different regions will likely be necessary. Investigation into using spatial atmospheric model data, such as

NCEP reanalysis, that is globally consistent and can be assessed in an automated fashion to retrieve some of the atmospheric characteristics such as temperature, humidity, wind speed and direction is part of our future plans.

In order to access the MODIS HDF data the filenames must be known by the code. This is achieved by creating an ASCII file for each data file that lists all the corresponding filenames. Besides the six text files containing the different MODIS data filenames, a text file must be created listing the directory names that were made to store the MODIS data. These files must contain an ordered list of the exact filenames on successive lines. The order of all the filenames must be consistent in each of these files so that data from the same event is analyzed simultaneously. If they are not, an error in the program will occur since the code can not find files with names not stored in corresponding directories. Creating a long list of filenames is tedious using the *cut-and-paste* approach from a Window viewer. In Unix, this task is easily completed for the MOD03 files, for example, with the command:

```
ls -1 MOD03* > batch_MOD03.txt
```

This command will place the filenames starting with *MOD03* in an ordered list with each name starting on a new line in a file called *batch_MOD03.txt.*

After the input data has been stored and data files created correctly, this information must be hardcoded into the program. This includes the exact names of the data path, the text filename containing the directory list, and the six text filenames containing the MODIS HDF names. This information should be individually written in between the quotes in the following commands and will be treated as character strings by the code:

```
path = 'F:\MODIS Data\'
batch_dirname = 'batch_dirname_2007.txt'
batch_infile_MOD03 = 'batch_MOD03_2007.txt'
batch_infile_MOD04 = 'batch_MOD04_2007.txt'
batch_infile_MOD05 = 'batch_MOD05_2007.txt'
batch_infile_MOD06 = 'batch_MOD06_2007.txt'
batch_infile_MOD07 = 'batch_MOD07_2007.txt'
batch_infile_MOD35 = 'batch_MOD35_2007.txt'
```

It is important to note that the path must have backslash ‘\’ after directory name.

3.2.2 Output

The CSEA code produces two major types of output: text reports and binary spatial data. There are four text reports produced on contingency that certain switched are set to *on*. If the *stats-switch* is *on* then the following two files are created:

MODIS_stats_ *AOIname*.txt
MODIS_Excelstats_ *AOIname*.txt

The first file includes text along with the data values while the second file contains only numerical data values in a single line per event so that they may be systematically incorporated into an excel spreadsheet. The variable *AOI_name* is a user defiend string representing the Are-of-Interest (AOI) chosen. These text reports contain the bulk mean and standard deviations of the MODIS derived cloud and clear-sky properties that are calculated for each event only for data inside the AOI. If the *analysis-switch* is *on* then the following two files are produced in the same manner as the statistics files:

MODIS_Cloud_Analysis_ *AOIname*.txt
MODIS_Cloud_Analysis_excel_ *AOIname*.txt

These two contain the results pertaining to the estimated cloud SLW and the total surface site precipitation if the *ground-switch* is also *on*. Before the start of the big loop these text files are defined and opened at the location defined by the *path* variable. As the statistics are calculated in each pass through the loop, they are written to the text report files. After the loop is finished and all the events have been analyzed, bulk property temporal means are calculated and written to the text files before they are closed.

The second output type is spatial data. After all MODIS data are read and aggregated, if need be, the AOI mask is applied that leave only the pixilated data in the AOI alone. All data outside the AOI are set to zero. These modified datasets are saved as binary files of appropriate data type. Scientific data is stored as floating point numbers while masks, flags and categorized data are stored as bytes or integers. Header files that contain the pertinent meta-data for each binary file are also created. These header files are made in a specific format for automatic file staging by the Environment for Visualizing Images (ENVI) software, a commercial remote sensing utility or Graphical User Interface (GUI) coded in IDL. As new datasets are created, they are also saved in the same format. These files are saved in the individual event MODIS data directories. The screen capture in Figure 4 shows the list of all the binary files that are saved for a particular MODIS event. Accompanying each binary file (.bin) is a header file (.hdr). The MODIS date format is copied from the HDF input files and included in these output filenames. All the filenames also begin with the user defined string that is made to indicate the AOI chosen.

3.3 Algorithm Structure

The CSEA code structure and methodology is further described in the following seven subsections.

3.3.1 Controls

The user controls four different functional aspects of the program: filenames, process switches, AOI boundaries, and scientific parameters. The following filenames must be assigned in the following example lines of code:

```
path = 'F:\MODIS Data\'
batch_dirname = 'batch_dirname_2007.txt
batch_infile_MOD03 = 'batch_MOD03_2007.txt'
batch_infile_MOD04 = 'batch_MOD04_2007.txt'
batch_infile_MOD05 = 'batch_MOD05_2007.txt'
batch_infile_MOD06 = 'batch_MOD06_2007.txt'
batch_infile_MOD07 = 'batch_MOD07_2007.txt'
batch_infile_MOD35 = 'batch_MOD35_2007.txt'
precip_path = path
precip_infile = 'NM_Precip_accum_diff_2007.txt'
```

The *path* variable holds the machine location where the ASCII files and the MODIS data directories are located. The *batch* variables are the filenames of the ASCII files that contain the order lists of the MODIS data directories and MODIS HDF files. The *precip_infile* variable is the name of the ASCII files that contains the ground site geo-location and precipitation daily accumulation data. The *precip_path* variable makes it possible to place the ground data files in another location.

The following nine switches should be set based on the data availability before the program is run:

```
MOD04_switch = 1
MOD05_switch = 1
MOD06_switch = 1
MOD07_switch = 1
MOD35_switch = 1
GS_switch = 1
stats_switch = 1
analysis_switch = 1
val_switch = 0
```

A value of 1 means that the function is turned *on* while a 0 value means that it is *off*. The six MODxx switches dictate whether the individual MODIS HDF files are examined or not. It should be stated that at the very minimum, the MOD03, MOD06, and MOD35

files need to be utilized so that cloud properties, including cloud SLW, can be determined. The *GS_switch*, *stats_switch*, and *analysis_switch* control whether surface data, bulk MODIS cloud and clear-sky properties, and cloud SLW estimations are performed, respectively. The *val_switch* determines whether the CSEA derived properties will be compared to CloudSat data.

The following string variable and four numerical geo-location values should be given (geo-location in floating point) by the user:

```
AOI_name = 'NM'
AOI_lat_bound_north = 37.0
AOI_lat_bound_south = 31.33
AOI_lon_bound_west = -109.0
AOI_lon_bound_east = -103.0
```

The values given above approximated the state boundaries of New Mexico and thus the abbreviation NM was used as the *AOI_name*. Care must be taken to insure the geo-location values are consistent with MODIS format. This means that latitudes in the northern hemisphere are positive while those in the southern hemisphere are negative. In addition, western hemisphere longitudes are negative and eastern hemisphere longitudes are positive. It would also be wise for the user to insure that the chosen AOI are included in spatial extent of most of the MODIS granules. Constant boundary values producing rectangular AOI is currently the only possible format.

The last set of user controls consists of the scientific threshold parameters employed for the determination of the cloud SLW. These variables and their default values are given in the subsequent list. The parameter unit is shown after the semicolon, which is the symbol used in IDL to begin written comments.

```
COD_min_thres = 1.0
CloudThickMax = 20.0              ; km
CTT_max_thres = 275.0             ; Kelvin
MoistAdiabaticLapseRate = 6.0     ; K/km
SCLW_min_thres = 200.0            ; K
SCLW_max_thres = 273.0            ; K
```

All of these parameters likely have a pronounced effect on the estimation of Cloud SLW content in various ways. These default values were chosen because they are both realistic and provide insurance against producing extreme values. The *COD_min_thres* parameter limits the calculation of cloud SLW to clouds that possess optical depths greater than a certain amount. This, in essence, eliminates the thinnest cloud. The concern is that the algorithm may overestimate the cloud thickness and, thus, the cloud SLW for thin clouds. It is also assumed that cloudy pixels with low optical depth are more than likely either partially filled pixels (cloud edges) or thin cirrus, which are primarily made of ice particles. Sensitivity studies were performed by varying this parameter to measure its cloud SLW estimation effect and are presented in a later section.

The *CloudThickMax* variable limits the calculation of cloud vertical thickness. This is used as a safeguard so that unrealistic values will not accidently be used, but also as a quick way to regulate this calculation. It was set to the very large number of 20 km so that the cloud thickness parameterization could be fully examined. The general default value was 7 km. Only cumulonimbus clouds would exceed the 7 km mark, and it is difficult to determine the cloud particle phase in these very dynamic thunderstorms. In the future, we will limit cloud thickness by calculating the vertical distance between the known surface elevation and the calculated cloud top height from retrieved cloud top temperature. In the current version of the algorithm, it is possible to produce clouds that extend below the ground.

The *CTT_max_thres* determines which cloud pixels should be examined for SLW. Any cloudy pixel possessing a cloud top temperature (CTT) above this value is not examined since it would be too warm to contain any SLW. A threshold near the freezing point is an appropriate value since cloud temperatures are expected to increase with decreasing altitude. The slightly above freezing value of 275 K was used because CTT is often overestimated due to cloud emissivity values less than unity.

The *MoistAdiabaticLapseRate* parameter determines the rate of temperature increase with decreasing elevation and is defined in K/km. This is used with the cloud vertical thickness to determine an estimate of the cloud base temperature. As a result, it defines the cloud temperature range and, thus, the potential cloud SLW layers. The value of 6 K/km is a standard moist lapse rate, but actual lapse rates are know to vary substantially from as low as 2 K/km to 8 K/km depending mostly on water content which controls the amount of latent heat released in moist air (cloud) parcels. Linking this parameter to liquid water content or clear-sky water vapor concentration is still being investigated.

The final two parameters, *SCLW_min_thres* and *SCLW_max_thres*, define the limits in temperature for which cloud SLW can be estimated. No SLW estimations are made for cloud temperatures that fall outside these boundaries. The freezing temperature marks the maximum, while the 200 K value (-73º C) is a conservative temperature for which only ice particles are expected to exist.

All of the variables under user control are found near the beginning of the main program. As a result, care must be taken to find them all. In the future, these control variables will be stored in a separate header file that will be automatically included in the program in order to provide greater clarity to the user.

3.3.2 Subroutines

The program calls the three subroutines to do specific tasks:

envi_output.pro
cloud_thickness_est.pro
cloud_LW_frac_est.pro

These are written as part of the same file, so they are compiled at the same time as the main program. The *envi_output.pro* routine accepts a dataset, a complete filename with path, and a string descriptor and produces a binary file and a header file. This program is called to output every spatial dataset. The *cloud_thickness_est.pro* routine returns the parameterized cloud thickness given cloud top temperature and optical depth. This routine is called for each individual confident cloud pixel. The *cloud_LW_frac_est.pro* subroutine returns the mean column cloud liquid water fraction of the potential SLW cloud layer. This routine only needs the minimum cloud SLW temperature and the number of unit temperature intervals (K) defined from the minimum to the maximum temperature of the cloud SLW layer. These were calculated using the cloud top temperature, the cloud thickness estimation, and the user defined SLW temperature limits. The specific methodologies of these parameterizations are given in subsequent sections

3.3.3 Reading Data

The first data files that are read are the ASCII files containing the ordered MODIS data directory and MODIS HDF file lists. Once each user given filename is concatenated with the *path*, the number of lines in each files is determined with the IDL command *FILE_LINES*. A string array is then created into which the filenames are read. The specific MODIS file lists that are read are determined by the control switches. If the *GS_switch* is set to *on*, then the surface data, precipitation accumulation only at this point, is read. Once the path is concatenated with the *precip_infile* filename, the data are read at one time using the IDL *READ_ASCII* command. The data dimensions are determined and arrays are created to store the ground site latitudes and longitudes and the event data.

The first function inside the algorithm loop acquires the MODIS data contained in the HDF files. Again, the data switches control which specific MODIS files are read. MODIS filenames are first concatenated with the *path* and their corresponding directory name. Special procedures and commands are needed to open, find, and read HDF data. Using the special IDL commands, HDF files are accessed in Read-Only mode and the dataset ID is found using the dataset character name that is hard-coded into the program. This makes it invisible to the user, but also makes it difficult for the user to read in different data if so desired. Then the dataset is selected and the data are read into a two-dimensional array, after which access to dataset is formally ended. This process continues for each dataset in the HDF file before formally terminating access to the HDF file.

3.3.4 Geo-location

Geo-location is given by the MODIS 1 km latitude and longitude from the MOD03 HDF file. All MODIS spatial data exists in this defined space. The reason to work in this space is to maintain the spatial quality of the data as best as possible. Translating the MODIS derived products to an arbitrary grid would require data averaging and

smoothing. From the MOD03 datasets, spatial data dimensions for 1 km are given and dimensions for 5 km and 10 km resolutions are calculated. On occasion some of the dimensions of other MODIS datasets are not consistent with the MOD03 geo-location datasets. This will cause an error and the program will be suspended. There is no fix for this data inconsistency except to remove the bad data file from the processing queue.

An AOI mask is created to identify pixels inside the user-defined area-of-interest. It is made at 1 km resolution by setting the values to 1 for pixels with geo-location values within the AOI limits and setting other pixels to 0. Latitude, longitude and AOI mask fields are then constructed at 5 km and 10 km resolution by sampling the data. This process will be described in the next subsection. The latitude and longitude fields are multiplied by the AOI mask at each resolution which zeros-out the data outside of the AOI. This function is performed for all MODIS datasets in order to easily exclude data from outside the AOI from being examined. Lastly, the number of pixels in the AOI at each resolution is determined for later statistical use.

3.3.5 Data Aggregation

It is necessary to aggregate a data field when the data are required at a lower resolution. The latitude, longitude and AOI mask fields at 1 km resolution are degraded to 5 km and 10 km by sampling. When 1 km pixels are grouped into successive n pixel x n pixel groups, the middle pixel is used to determine the entire group value. To create the 5 km resolution field, the pixel value in the third column and third row of each 5 pixel x 5 pixel group is taken to represent the entire 25 km^2 area. For the 10 km field, the pixel value in the sixth column and sixth row is sampled. The sixth pixel is not the exact middle pixel of the 10 x 10 group of pixels, but the slight offset is not expected to produce any serious errors.

Scientific data are aggregated by averaging. The four cloud properties fields of effective particle size, optical depth, water path and water uncertainty at 1 km resolution are used to create 5 km resolution fields by simply taking the mean of successive 5 pixel x 5 pixel groups.

Integer data that utilize whole numbers to represent certain results must be handled differently because sampling and averaging will not necessarily produce representative values. The 1 km cloud multilayer flag field is degraded to make a 5 km field. This data consists of integers from 0 to 9, with 0 and 1 representing no cloud and single-layer cloud, respectively. All higher values represent some sort of multilayer cloud with the value of 2 being of very low confidence. Since the primary importance is whether a single layer or multilayer cloud exists over the 5 pixel x 5 pixel domain, the focus is only on the difference between these groups of values. The number of data values of 1 and the number of data values greater than 2 (2 is ignored because of its low confidence) is counted from each group of 25 pixels. If the percentage of values equal to 1 is greater or equal to 90%, the 5 km x 5km pixel is given the value of 1. Similarly, if the percentage of pixels with values greater than 2 is greater or equal to 90%, the 5 km x 5 km pixel is

set to 3. If neither of these conditions is meet, the 5 km x 5 km pixel is given a value of 2.

The 1 km resolution cloud mask from the MOD35 file is stored as a bit flag, meaning that individual bits represent certain environmental characteristics and test results. The cloud confidence data is stored in the first byte. After extracting these bits, the cloud confidence data value is saved. Cloud confidence is binned into four categories with the following data values: confident cloud (0), likely cloud (1), less likely cloud (2), and confident no cloud (3). Reducing the cloud confidence resolution focuses only on the two confident states of cloudy and no-cloud (clear) because these states will determine which pixels are used when deriving properties and statistics. The number of confident cloud pixels and confident clear pixels are determined from the 25 pixel and 100 pixel groups for 5 km and 10 km resolution fields, respectively. If the percentage of pixels with a confident cloud value of 0 is greater or equal to 90%, then the lower resolution pixel is set to 0, or confident cloud. If the percentage of pixels with a value of 3 is greater or equal to 90%, then the lower resolution pixel is set to 3. If neither of these conditions is meet, then the lower resolution cloud mask pixel is set to 1. As the resolution decreases the number of 1 km pixels that are used to produce the new filed increases. At 10 km resolution, the 90% single confidence type condition becomes more difficult to achieve. Therefore, the 10 km cloud masks may seem to have more pixels in limbo, with a value of 1 than the better resolved cloud mask fields.

3.3.6 Spatial Statistics

The user decides if the program will generate mean spatial statistics for each event it analyzes by setting three switches. If the *stats_switch* is set to *on*, then statistics are produced for all of the MODIS datasets of interest listed in Table 1. Mean statistics are produced only from the AOI defined. Mean cloud and clear-sky statistics are made only from confident cloud pixels and confident clear pixels, respectively, as defined by the cloud mask. In addition, the *MOD03_switch*, *MOD06_switch*, and *MOD35_switch* need to be set *on* before the cloud statistics are calculated. This is a safeguard since these cloud products are needed to generate the cloud statistics. For clear-sky statistics to be derived the *MOD03_switch* and *MOD35_switch* must also be set to *on* since geo-location and clear-sky confidence are obtained from these files. The *MOD04_switch*, *MOD05_switch*, and *MOD07_switch* must also be set to *on* to generate clear-sky statistics for the products that these files contain. These statistics are written to the text file named *MODIS_stats_ AOIname.txt* and annotated with appropriate descriptions. Certain statistics, but not all, are also written to the *MODIS_Excelstats_ AOIname.txt* without text annotation. Rewriting specific lines of code is necessary if a change in the property statistic output is desired. Temporal means for each property are also written to the text files so that these longer-term averages can be compared to other periods.

Derivation of new cloud properties is controlled by the *analysis_switch*. The following spatial new cloud properties are derived and saved as binary files:

Cloud thickness

Cloud SLW mask
Cloud SLW mass
Cloud SLW fraction

Cloud thickness is the parameterized pixel cloud vertical depth. The cloud SLW mask identifies pixels that contain some super-cooled liquid water. The Cloud SLW mass is the estimated mass of the super-cooled liquid water portion of the cloud. The cloud SLW fraction is the fraction of the cloud mass that is estimated to be in the super-cooled liquid water phase. A more detailed description on the methodology used in determining these properties is given in the next section. These four cloud properties along with the MODIS derived cloud water path uncertainty are written to the two text files named *MODIS_Cloud_Analysis_AOIname.txt* and *MODIS_Cloud_Analysis_excel_AOIname.txt*, with extra written annotation included in the former file. Temporal means are also produced for these new cloud properties and written to the text files. If the *GS_switch* is also turned *on*, precipitation accumulation for all ground sites inside the defined AOI are summed and written to the two text files as well.

3.3.7 Cloud Super-Cooled Liquid Water Estimation

Estimation of cloud super-cooled liquid water is made only if the *analysis_switch* is set to *on*. It is made on an individual pixel basis at 5 km resolution if the following three criteria hold true:

1. Cloud mask is *not* confident clear.
2. The cloud optical depth is greater that a certain minimum value.
3. The cloud top temperature is less than a certain threshold near the freezing point.

The first condition removes only the confident clear pixels. Less confident cloud pixels are not eliminated. The rationale is to not constrain the initial condition too greatly. Non-clouds, cloud edges, and thin clouds can be removed by the next two criteria. These last two criteria are sensitive to user control. The second condition reserves the estimation of cloud SLW to clouds of certain optical thickness. The last condition is designed to eliminate warm clouds with top temperatures above the freezing mark, since these will contain no SLW. For pixels that meet these three criteria, new derived cloud properties are determined.

The estimation of cloud vertical thickness is the first step in the process. Cloud top temperature and mean cloud optical depth at 5 km is passed to the subroutine *cloud_thickness_est*. The following parameterization for vertical cloud thickness, Δz, in km, from Minnis et at. (1995) is used:

For $T_c < 245$ K, $\Delta z = 7.2 - (0.024*T_c) + (0.95*\ln \tau)$ (1)
For $T_c > 275$ K, $\Delta z = 0.85*\ln \tau$
For $245 \text{ K} < T_c < 275$ K, linearly interpolate Δz between 245 K and 275 K.

In the statements above T_c is the cloud top temperature and τ is the cloud optical depth. Figure 5 shows the parameterized cloud thickness values as a function of cloud top temperature for three cloud optical depth (COD) values. For the same optical depth, cloud thickness increases with decreasing cloud top temperature. This is consistent with the general rule that warm clouds of liquid phase require less thickness to achieve the same optical depth (at 0.5 µm) than cooler mixed or ice phase clouds. As optical depth increases for the same cloud top temperature, the estimated cloud thickness increases as one would expect. After the estimated cloud thickness is returned it is compared to the user defined *CloudThickMax* variable. If the parameterized variable is larger than the user maximum then the cloud thickness is set to the *CloudThickMax* value. New cloud thickness estimations based on cloud type and phase may provide more accurate values (Chakrapani et al., 2002), but are not included in the CSEA code because of the difficulty in accurately characterizing the cloud type.

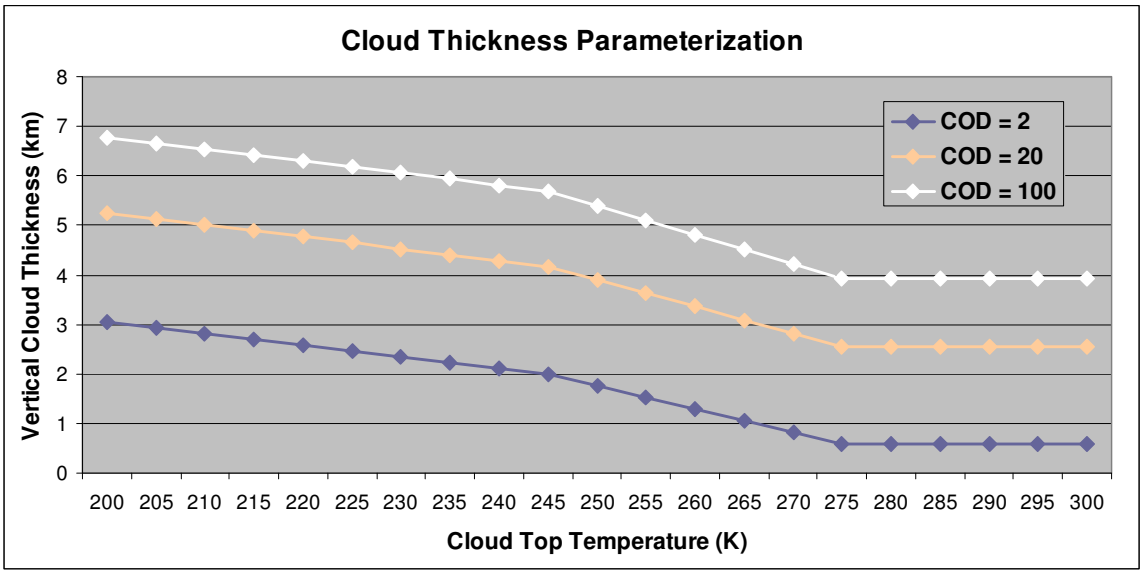

Figure 5. Cloud thickness parameterization as a function of temperature following Minnis et al. (1995).

In preliminary program runs with several different constant cloud thickness values imposed, cloud SLW potential estimates were seen to vary as cloud thickness changed. Figure 6 shows the total potential cloud SLW volume for a 10 event period in 2007 over New Mexico for increasing assumed cloud thickness (dz) values from 1 km to 4 km. Some events show very little variation in total cloud SLW volume when the cloud thickness is changed. On other days, total cloud SLW water appears to linearly increase with cloud thickness. There is a cloud top temperature dependence that is primarily responsible for the different volume rates of change with cloud thickness. At the same time, it is apparent that an incorrect cloud thickness approximation can often lead to large errors in cloud SLW. Cloud thickness sensitivity tests are described in more detail in a later section.

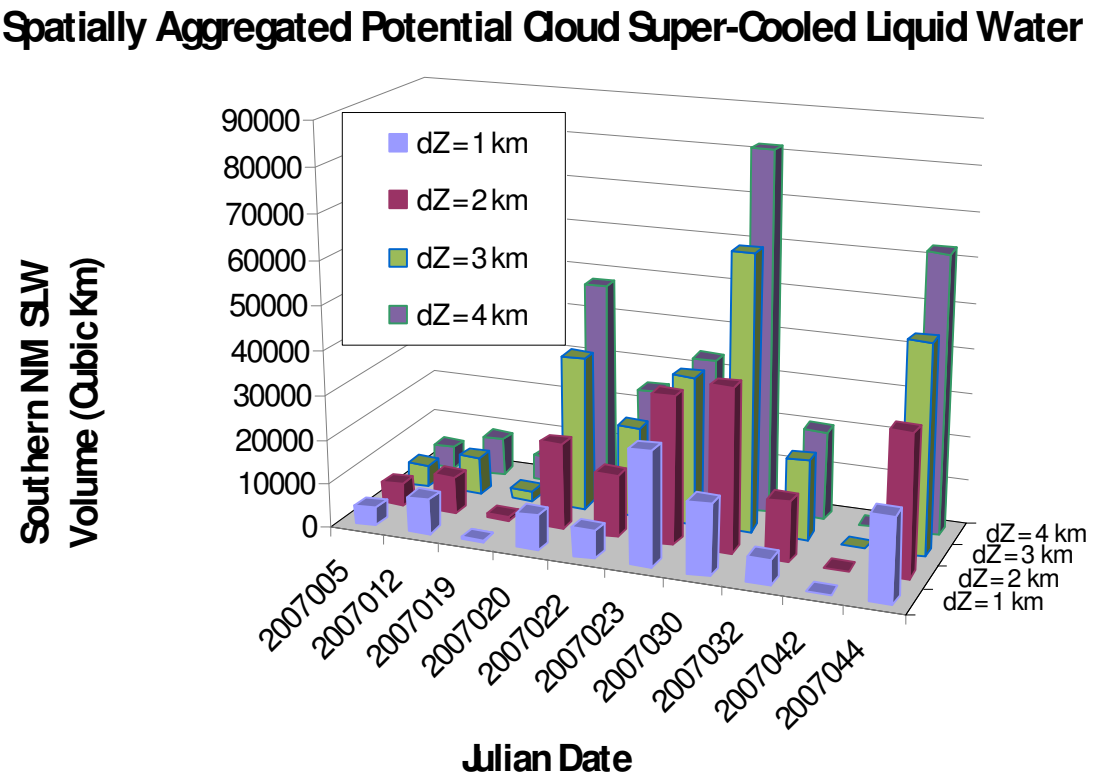

Figure 6. Estimated cloud SLW potential volume over southern New Mexico as a function of cloud vertical thickness during the beginning of 2007.

The temperature of the cloud based is derived using the MODIS cloud top temperature and increasing the temperature by the product of the *MoistAduiabaticLapserate* value and the cloud thickness estimate. This cloud temperature range is noted. Using the cloud top and base temperatures along with the *SCLW_max_thres* and *SCLW_min_thres* temperature limit variables, the cloud SLW temperature range is calculated. The number of whole degree temperature units is found by rounding the cloud SLW temperature range to the nearest integer. If the cloud contains any temperatures within the cloud SLW temperature range then the cloud liquid water fraction for this temperature range is derived. The minimum cloud SLW temperature and the number of whole temperature units in the SLW layer are passed to the subroutine *cloud_LW_frac_est* to perform this calculation. The routine loops through the SLW temperature range one degree at a time starting with the minimum value that was passed. At each temperature the fraction of liquid cloud water as opposed to ice content is calculated and stored. After these calculations are performed the mean liquid water fraction is determined and returned to the main program. Cloud liquid water fraction is parameterized as a function of cloud temperature using a hyperbolic tangent function. This parameterization of thermodynamic phase is of standard use in certain general circulation models (GCM) and by the POLDER satellite-based algorithms that retrieve cloud phase (Doutrriaux-Boucher and Quaas, 2004). The equation utilized for the parameterization of liquid water fraction, X_{liq}, is as follows:

$$X_{liq} = ½(1 + \tanh(a_1 * T + a_2)), \quad (2)$$

where $a_1 = 0.1$ and $a_2 = -25$. These values were chosen to produce a 50% liquid water fraction at 250 K and tails near 100% and 0 % at the freezing point and -50° C, respectively. The liquid water fraction equation is graphical displayed in Figure 7.

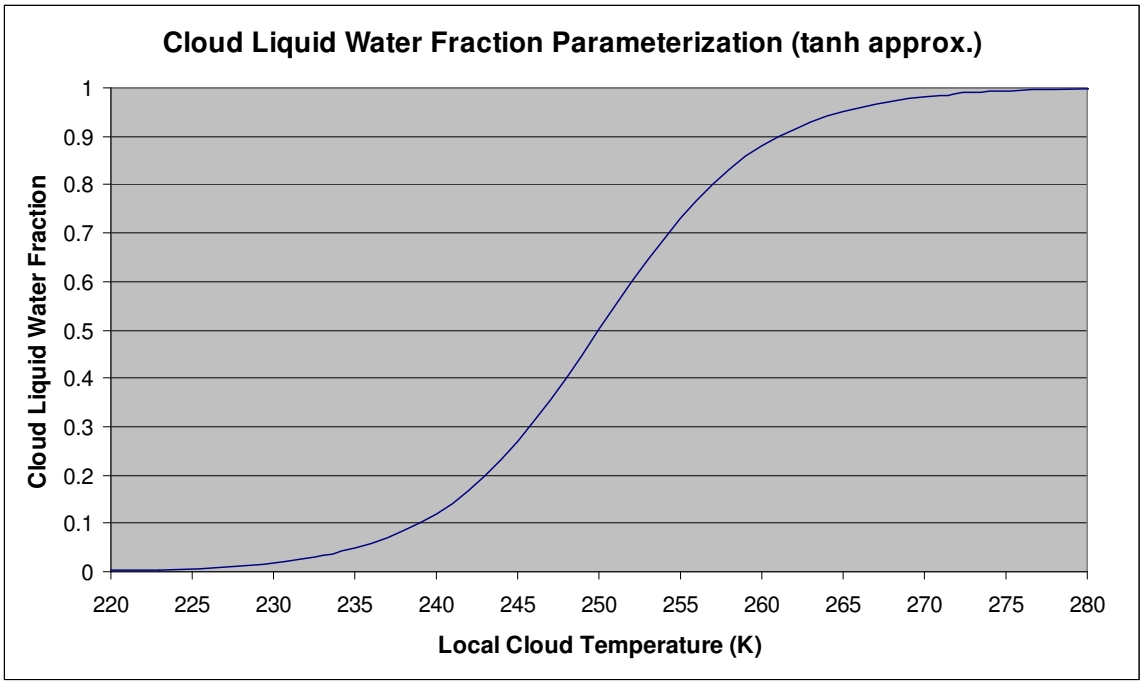

Figure 7. Parameterization of cloud liquid water fraction versus temperature.

The total cloud fractional SLW, is calculated in two steps. The product of the parameterized mean fractional SLW in the SLW layer and the temperature range of the SLW layer produces an approximation of the fraction of liquid water in the SLW layer only. This product divided by the total cloud temperature range approximates the SLW fraction of mass in the entire cloud. The main assumption is that cloud particle density is constant throughout the vertical layer. This assumption is not true for thick cloud layers due to large pressure variation from the cloud top to the cloud base, but if the SLW layer is near the middle of the cloud or runs throughout the entire vertical depth of the cloud, then this approximation is reasonable. This cloud SLW fraction is then multiplied to the MODIS derived cloud water path (CWP) to give an estimate of the cloud SLW path on a 5 km horizontal scale. The MODIS produced CWP uncertainty is used as an estimate of the uncertainty for the new cloud SLW path value. This value over-estimates the cloud SLW uncertainty if the cloud SLW fraction is small. Since an error budget for the SLW estimation has yet to be complete, the given CWP uncertainty is used in its place. Cloud SLW mass, in kg, is determined for each pixel by using the 5 km x 5 km dimensions and the column SLW estimation. This SLW mass value is also summed across the AOI to produce a regional quantity.

4. RESULTS

Results were generated for the 81 cases that were identified as having more than 30% cloud coverage in either the northern or southern half of the state of New Mexico using GOES visible and LWIR imagery. This means that a minimum of 15% of the entire state possessed detectable cloud. The MODIS data obtained from the Terra satellite was collected within the hour of the GOES data. Cloud coverage may have changed somewhat during that time. At the same time, MODIS cloud detection is sophisticated compared to that of the simple two band GOES method described in Roskovensky et al. (2009). In most cases, MODIS detected significant cloud which provided a good dataset for the quantification of cloud SLW. The state of New Mexico provided the boundaries for examination. Table 4 lists the exact latitudes and longitudes of the approximate state corners that were used to define the AOI. Due to the non-rectangular shape of the state, the southeast corner of the AOI actual includes a small part of the state of Texas.

Table 4. Geo-location approximations for New Mexico.

Parameter	Value
New Mexico NW corner latitude	37 º N
New Mexico NW corner longitude	109 º W
New Mexico NE corner latitude	37 º N
New Mexico NE corner longitude	103 º W
New Mexico SW corner latitude	31.33 º N
New Mexico SW corner longitude	109 º W
New Mexico SE corner latitude	31.33 º N
New Mexico SE corner longitude	103 º W

This section provides examples of the spatial data and mean statistical properties produced by the CSEA program. Temporal statistics are also examined and certain retrieved property correlations are presented. Results from a smaller AOI centered over Taos, NM and the Sangre de Christo Mountains is also presented. Algorithm sensitivity studies, which focus on several critical parameters, were performed and are discussed.

4.1 Spatial Data

Spatial data from the cloud event on 6 October 2006 (Julian day 279) is examined in depth in this subsection. Figure 8 show the MODIS true color image with the approximate position of the New Mexico AOI overlaid with a red-lined boundary. The entire NM AOI is contained inside the MODIS Granule. There appears to be substantial cloudiness in the western part of the state. Clear-sky areas are also apparent in the southeastern section. This example will provide the basis to show both cloud and clear-sky properties.

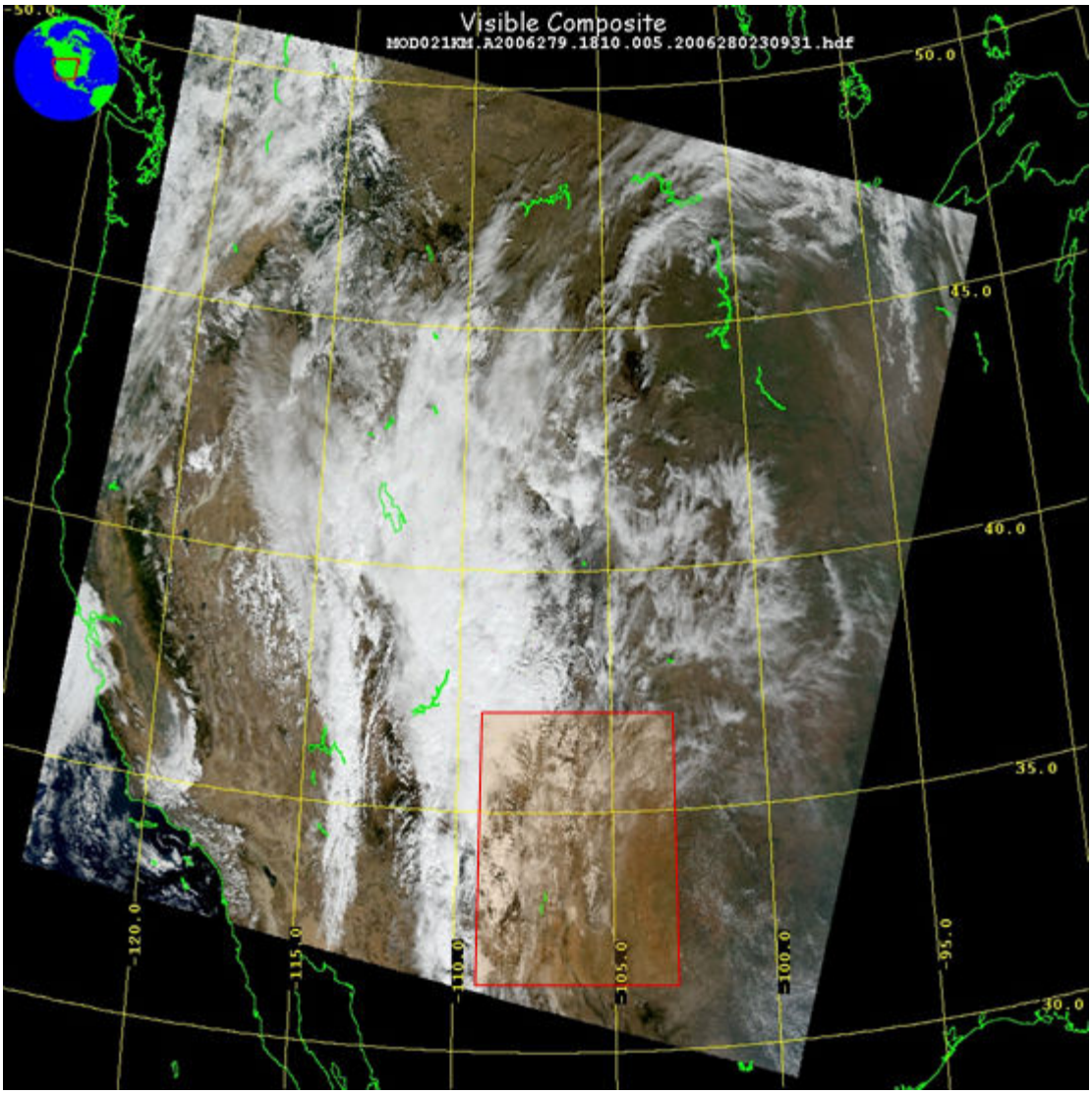

Figure 8. MODIS (Terra) true color granule image on 6 October 2006 (1810 UTC), with approximate New Mexican region superimposed.

Figure 8 displays the MODIS granule laid on a map projection. The CSEA code works in MODIS data rectangular space defined by the number of samples as the column, and the number of scan lines as the row dimensions, respectively. The leftmost image in Figure 9 shows the three-color (true-color) image at 1 km in MODIS rectangular space with the New Mexico AOI boundaries superimposed. The state area takes only a small fraction of the entire MODIS granule. Based on this true-color image, it is apparent that the thickest clouds of the large cloud field lay to the northwest of New Mexico and that thin cloud seems to cover the majority of the central part of the state. The middle image in Figure 9 is a zoomed-in MODIS true-color image focused on the New Mexico AOI mask. From this image it is easy to see that the thickest clouds in the AOI are along the western state border. The rightmost image in the figure shows the actual binary zoomed-in AOI mask with 0 and 1 representing non-AOI and AOI pixels, respectively. The rest of images included in this section are in the zoomed-in scale.

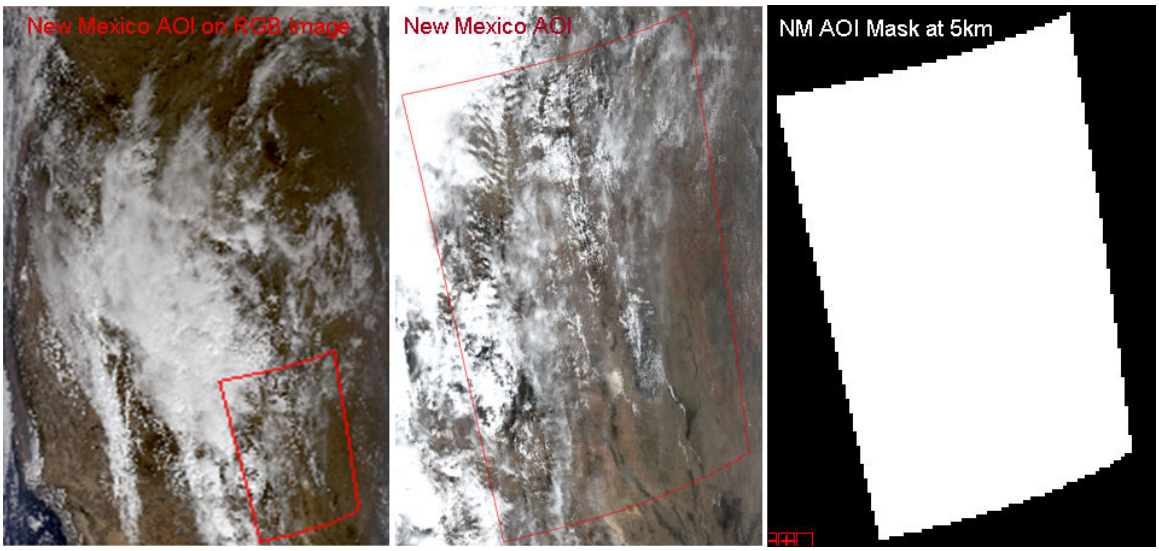

Figure 9. True color image (left), zoomed-in true-color image (center), and zoomed in New Mexico AOI (right) from the MODIS (Terra) granule on 6 October 2006 (1810 UTC).

The three images in Figure 10 are of aggregated 5 km resolution versions of the latitude, longitude, and modified cloud mask. The two confident cloud mask states of cloud and clear are seen along with the not-confident category containing all other less confident states. A great deal of confident cloud covers the AOI. The non-confident category pixels are seen along the confident cloud edges. The non-confident cloud mask pixels are widespread and likely made up of pixels with partial confident cloud, thin cirrus, and pixels of low-confident clear values. There are less confident clear pixels.

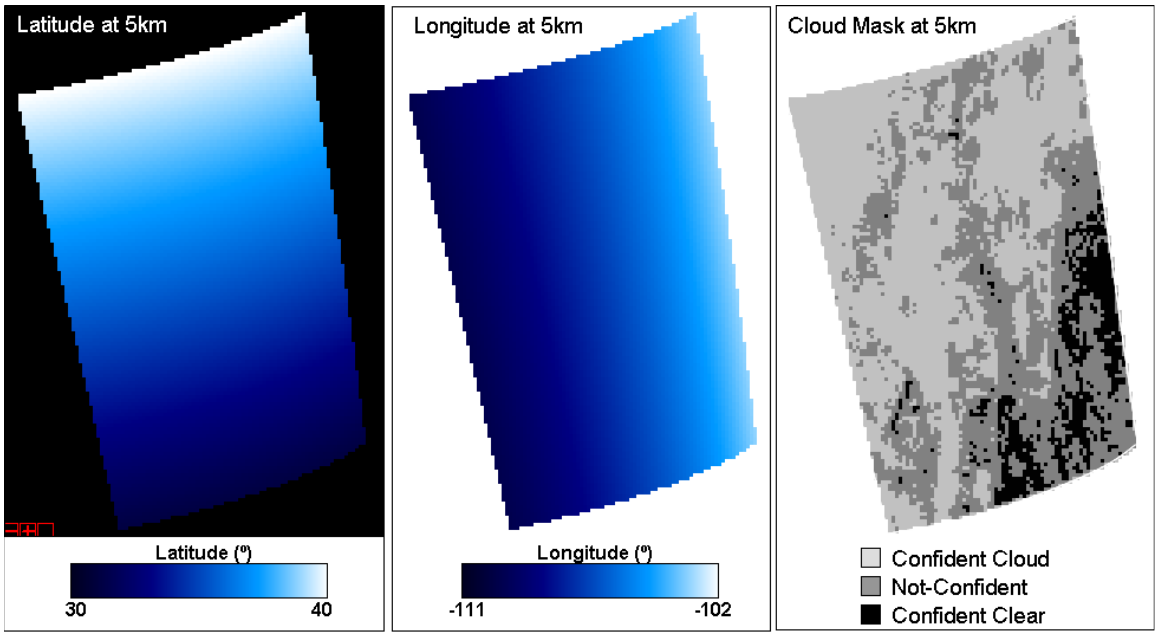

Figure 10. Same as Figure 9 except latitude (left), longitude (center), and cloud mask (right).

Figure 11 displays the MODIS derived cloud top temperature, the aggregated cloud optical depth, and the estimated cloud thickness at 5 km resolution, from left to right. The coldest cloud top temperatures (CTT) are generally aligned with the confident cloud of the cloud mask, but also identify the highest altitude clouds. The cloud optical depth (COD) image shows that the optically thickest clouds are along the western state boundary, very much in-line with the visibly bright clouds in the true-color imagery. These cloud areas are likely to possess the greatest cloud vertical thickness. The parameterized cloud thickness distribution depends on both the CTT and COD which is apparent from the derived thickness displayed in the image. The thickest clouds correlate to both high COD and low CTT values. Cloud thickness estimates of the thin cold clouds in the center of the AOI are probably too high. From the true color image, these clouds appear to be thin and semi-transparent, but because of their high altitude and, thus, cold top temperatures they are parameterized as vertically thick despite their moderate COD values. A parameterization scheme based on cloud type would likely be more accurate and will be studied.

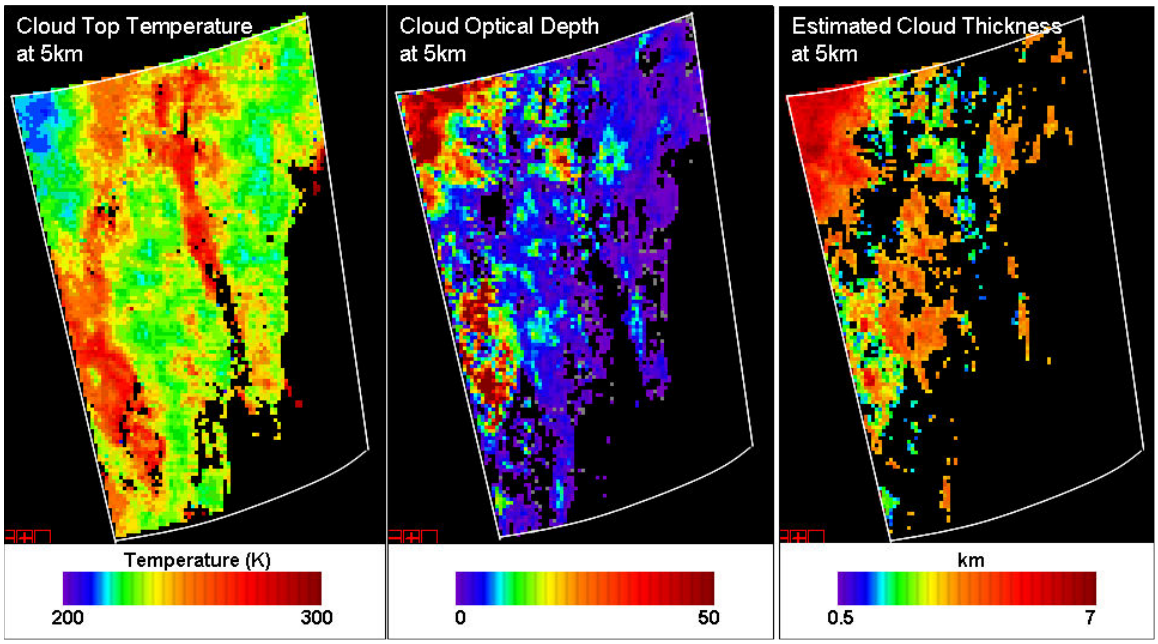

Figure 11. Same as Figure 9 except cloud top temperature (left), cloud optical depth (center), and estimated cloud thickness (right).

The next three images included in Figure 12 are of the MODIS derived cloud liquid water and its uncertainty (left and middle), and the estimated cloud SLW fraction (right). The cloud liquid water mimics the COD spatial distribution extremely well. The largest uncertainty values of cloud liquid water occur in cloud regions where the liquid water values are the greatest and along cloud edges where cloud confidence is lower. The cloud SLW fraction identifies the percent of the total cloud vertical temperature range that is within the SLW temperature range and is parameterized to be of liquid phase. Low cloud SLW fractions do not necessarily mean low quantities of cloud SLW. For example, vertically thick clouds that contain a great deal of SLW will possess a relative low fraction of SLW due to their large water content. In fact, the highest cloud SLW

fraction values for this event occur where CTT temperature are relatively high, indicating that lower-level cool clouds have a greater percentage of cloud SLW than high, cold clouds.

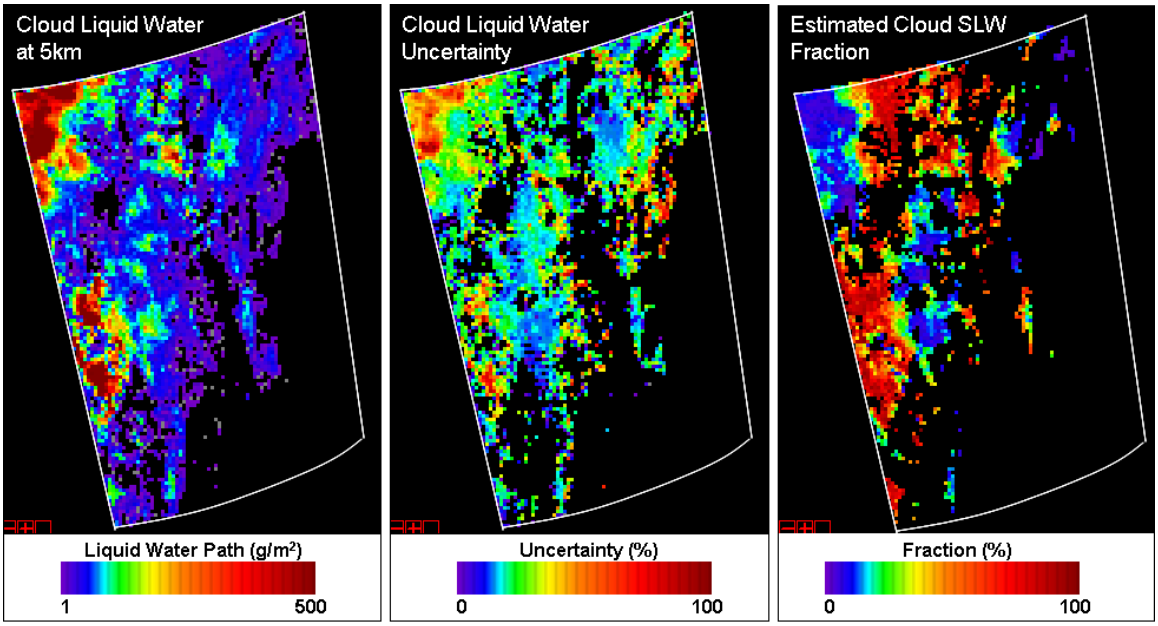

Figure 12. Same as Figure 9 except cloud liquid water (left), cloud liquid water uncertainty (center), and estimated cloud super-cooled liquid water fraction (right).

In Figure 13 the estimated cloud SLW mass per pixel at 5 km resolution or per 25 km^2 area is displayed in the leftmost image for the entire AOI. There are two regions where cloud SLW values are very large, more than 20 times that of the rest of the cloud regions. These high cloud SLW mass regions correspond to areas of large cloud liquid water, optical depth, vertical thickness, cloud SLW fraction and relatively warm cloud top temperatures at about 240 K – 250 K. Because this temperature lies just below the maximum parameterized SLW temperature range between 253 K and 273 K it is guaranteed to possess a great deal of SLW. The small image at the bottom of Figure 13 is a slightly zoomed-in portion of the main cloud SLW image identified by the red box. A horizontal profile of cloud SLW pixel data values through the 2-D field correlating to the horizontal red line in the middle of the small image is plotted in the graph (upper right). The large spike in estimated cloud SLW amount is apparent near the left end of the profile. The large difference in these highest estimates to that of the other cloud regions is noticeable.

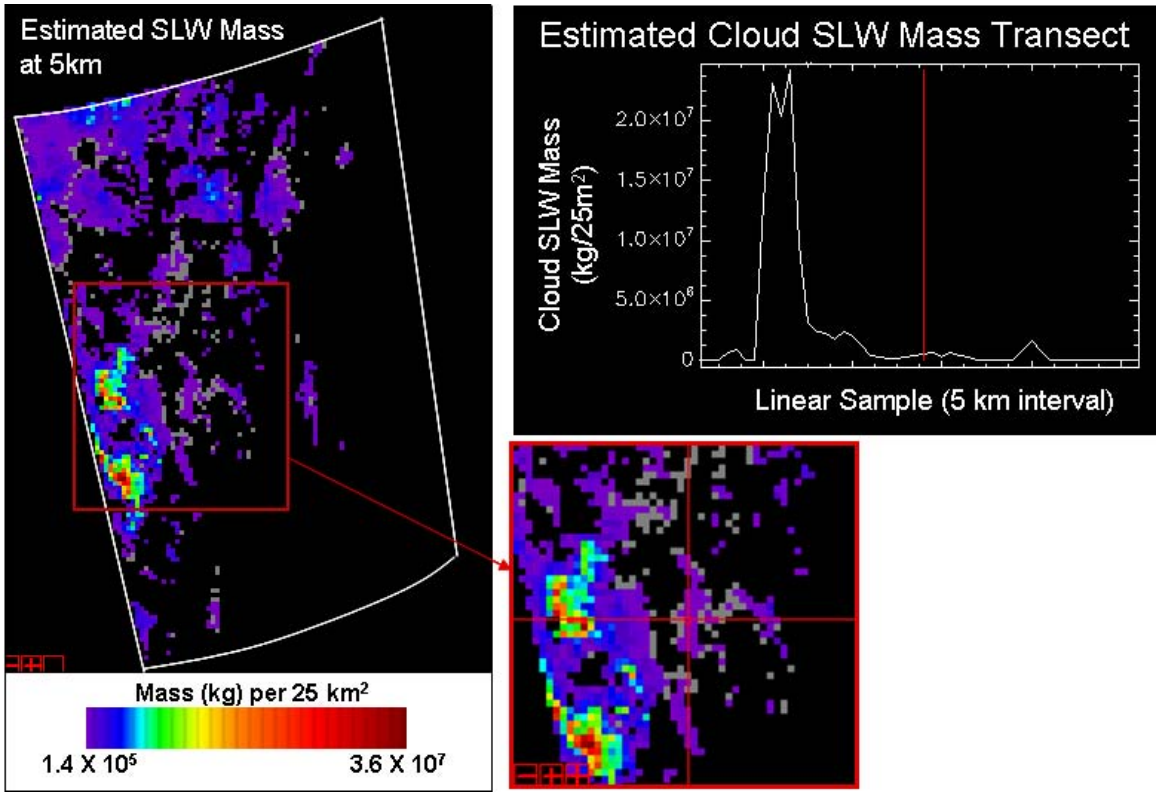

Figure 13. Estimated cloud super-cooled liquid water (left), zoomed in AOI region (lower right), and horizontal profile of cloud SLW in AOI (top right)

Further analysis of the MODIS data can aid in validating the cloud SLW estimates. Figure 14 displays the MODIS band-4 (left) and band-26 (right) reflectances at 1 km resolution for this event. Band-4 is located in the visible part of the spectrum with a center at 0.554 µm. Thick clouds are very reflective in this band regardless of their cloud top altitude. Cloud optical thickness is proportional to band-4 image brightness. Band-26 is centered at 1.38 µm, in a strong water vapor absorbing spectral region. Very little energy in band-26 from below the boundary layer, where most of the atmospheric water vapor exists, will be reflected to space. Therefore, the bright regions in the image are due to high-altitude clouds, well above the boundary layer. The band-26 brightness is proportional to high-cloud optical depth. For instance, the very bright clouds at the very edge of the image, outside the AOI, are cumulonimbus anvils that are at high-altitude and are optically thick. The relatively lower brightness of the cloud seen inside the AOI are likely thin cirrus with much lower optical depths. These cirrus clouds appear as moderate bright regions in the visible band, which supports the fact that they posses moderate optical depths. The two high estimated cloud SLW regions correspond to lower, warmer cloud with high optical thickness since they produce low band-26 reflectance and very high band-4 reflectance.

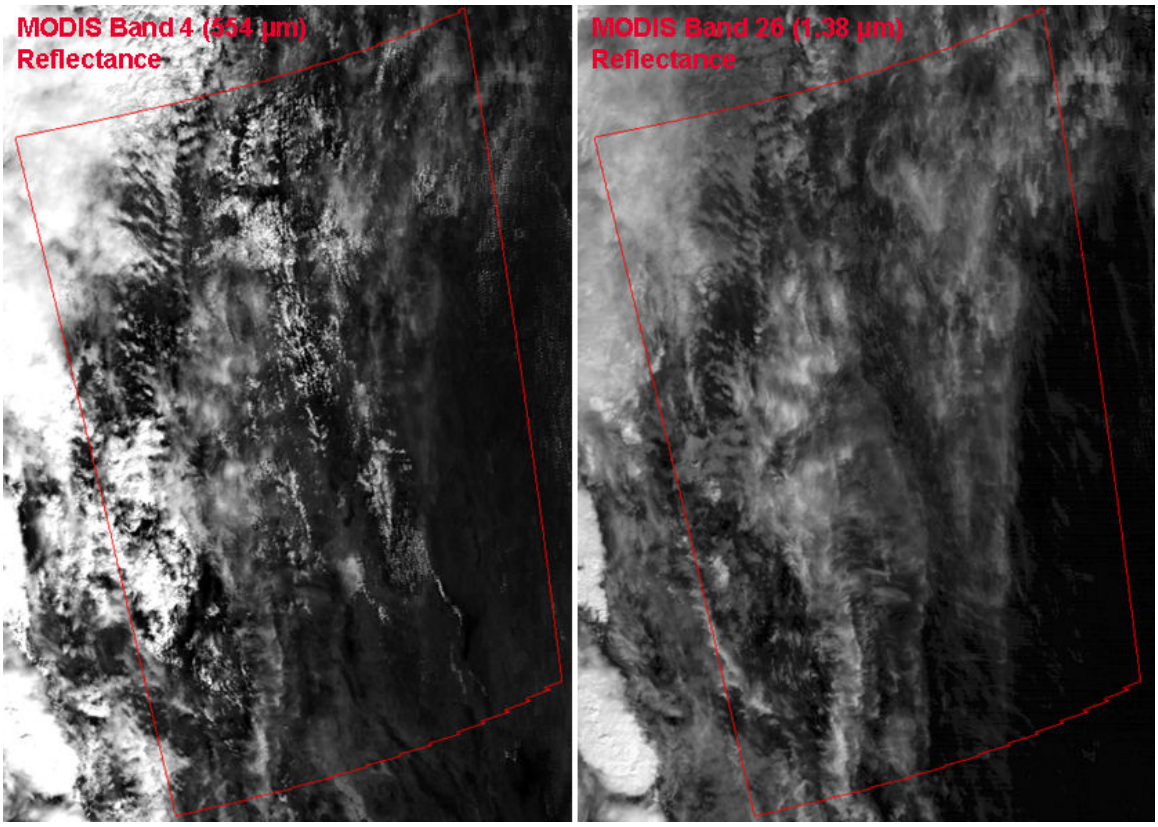

Figure 14. Same as Figure 9 except for MODIS band 4 (left) and band 26 (right) reflectance both with New Mexico AOI outlined superimposed.

Three interesting MODIS derived cloud products of cloud phase, cirrus flag, and multilayer flag shown in Figure 15 are not utilized by the CSEA algorithm. The cloud phase is derived by using brightness temperatures of three LWIR MODIS bands. According to the product technical document (Menzel et al., 2004) it accurately identifies either water, ice or mixed cloud about 80% of the time globally. The other 20% is considered uncertain. Most of the cloud cover inside the AOI is identified as ice phase. This ice distribution seems to compare well to the cirrus regions seen in the band-26 data and to the derived CTT values below 230 K. The large cloud SLW estimates are primarily associated with cloud phase determination of either mixed phase or uncertain phase. Mixed phase represents SLW layers. In this event the cloud phase could be used to help classify cloud types. The cirrus flag pixel setting is likely based on thresholding band-26 reflectance. From this product, cirrus clouds cover nearly the entire AOI. This seems to contradict the cloud phase ice distribution and seems to over-extend the cirrus cloud boundaries when examining the band-26 data. It is true that sub-visible cirrus is often widespread, but it is also true that band-26 will often show reflectance off of high terrain especially in areas of low water vapor concentration such as New Mexico. The striping seen in the image is produced by subtle calibration differences in the 10 scanning detectors. The multilayer cloud flag shows that the vast majority of the cloudy pixels are deemed to be of single layer. The colorful pixels represent some sort of detected multilayer cloud. The CSEA code assumes single layer cloud only so these pixels, if true, can cause errors in many of the derived cloud properties. Both the CTT and the

COD maybe affected by the lower cloud in a multilayer arrangement and produce falsely large values for the top layer cloud thereby increasing the estimated cloud layer. Eventually, multilayer cloud pixel may have to be excluded from processing.

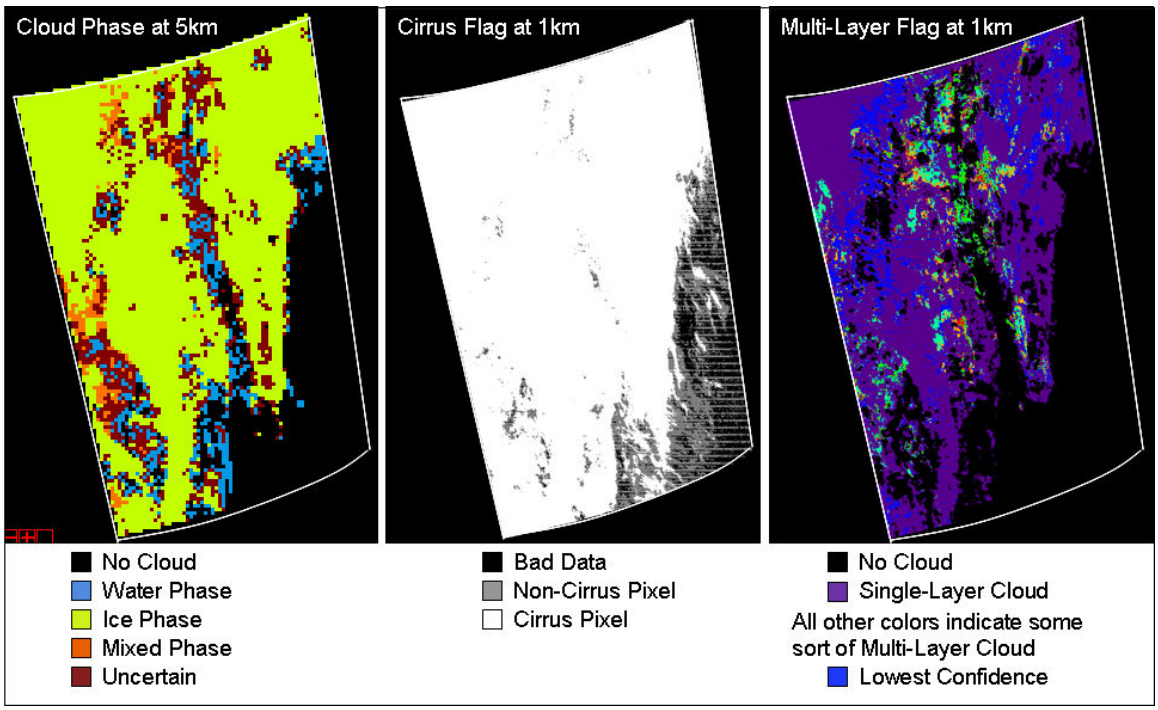

Figure 15. Same as Figure 9 except cloud phase (left), cirrus flag (center), and multi-layer cloud flag (right).

The clear-sky portion of the AOI is located in the southeastern section. Figure 16 shows the images of the MODIS derived aerosol optical depth (AOD), angstrom exponent, and lifted index. The first two properties describe the aerosol concentration and particle size distribution, while the latter is a measure for atmospheric stability. The lifted index clear-sky distribution does not always match that of the aerosol due to the differences in horizontal resolution and the aggregated cloud mask differences at those resolutions. The aerosol properties appear to be in the normal range with AOD between 0.1 and 0.3. The constant angstrom exponent value indicates that the retrieval algorithm more-or-less uses an expected value. The lifted index value of +4 K is indicative of a stable atmosphere (negative values represent instability). Both the AOD and the lifted index show enhanced and reduced levels, respectively, at the edge of the clear-sky regions. These are likely caused by cloud contamination due to thin cloud and/or partial cloud filled pixels. When calculating mean clear-sky statistics, only properties from confident clear regions are used. From the cloud mask at 5 km resolution in Figure 10, it can be seen that the actual confident clear-sky region is much smaller in area than the non-zero aerosol property regions. These less confident areas of the cloud mask likely contain a mixture of both clear-sky and cloud.

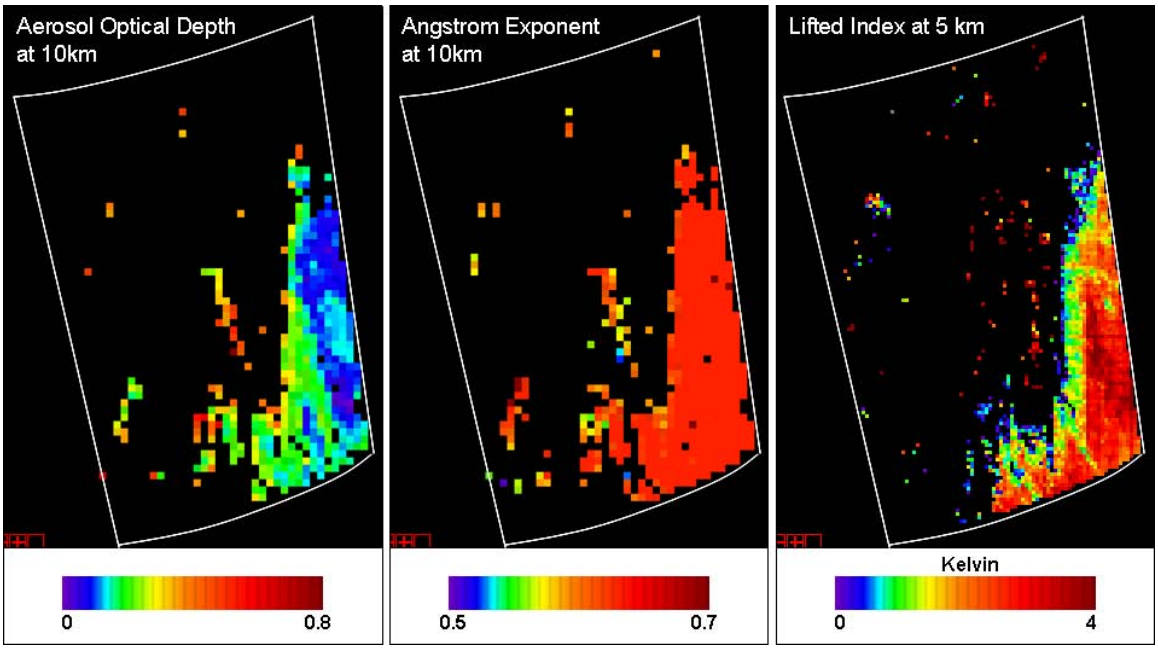

Figure 16. Same as Figure 9 except aerosol optical depth (left), angstrom exponent (center), and lifted index (right).

The two images in Figure 17 are the MODIS retrieved column water vapor. Each product relies on different methodology. The near-infrared (NIR) method utilizes reflected sunlight and differential absorption of two nearby bands. The infrared (IR) method used differential absorption of IR bands. Due to SNR considerations the IR product requires a 5 km resolution where the NIR is at 1km. The NIR method can retrieve water vapor above clouds and does not have any many zeroed out pixels. As is expected, the water vapor concentrations above the cloud regions are lower than the clear regions where water vapor is retrieved from the entire column. The IR product cannot retrieve water vapor above clouds which explains the zero values (black) areas. Comparing the clear-sky regions in the two products, it can be seen that the NIR retrieved values (2 cm – 2.5 cm) are larger than the IR retrieval (1.5 cm – 2 cm). It is not clear if this is due to a known bias or whether this is an anomalous event associated with the desert southwest or this time of year.

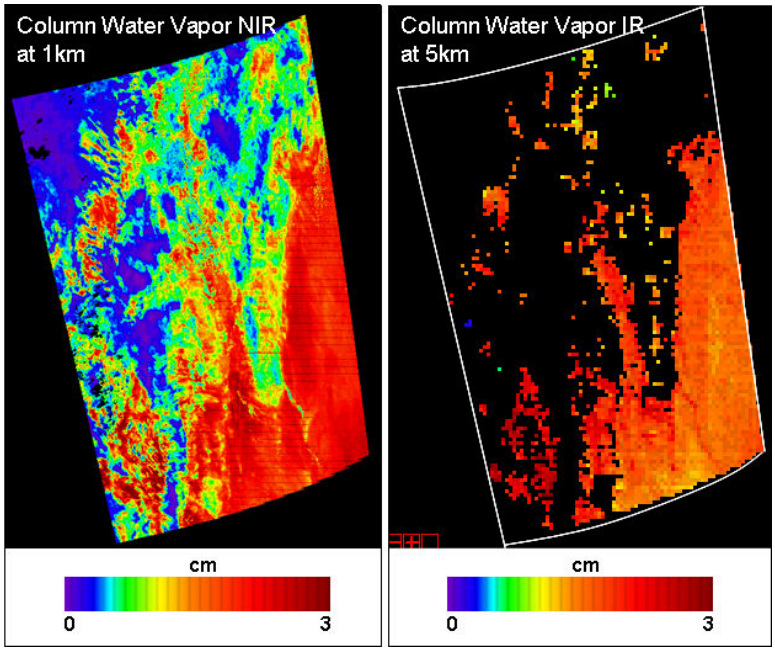

Figure 17. Same as Figure 9 except column water vapor retrieval from NIR method (left) and IR method (center).

In certain events the New Mexico AOI was not completely contained inside MODIS granule. For these cases the MODIS granule that possessed the largest section of the AOI was chosen and the data in that portion of the AOI were analyzed. The cloud event on 26 August 2006 (Julian day 238) is an example of this. The map projection of the MODIS three-color image on this day is shown in Figure 18. The superimposed box identifies the approximate location of the New Mexico AOI. Most of the AOI is contained in the MODIS granule, but the northern part of the state actually falls outside of the granule. Since the satellite orbits in either a north-to-south or south-to-north direction, data immediately to the north and to the south of any MODIS granule is continuous and can be used to form an instantaneous picture. Modification of the algorithm would be necessary to read in more than one granule per event in order to obtain higher spatial coverage of the AOI. Data to the east and west (right and left) of the MODIS granule are collected on a previous or later orbit, with a time difference of about 90 minutes. These data granules are not continuous in time or in space since there is often some overlap and gaps between the granule data from successive passes.

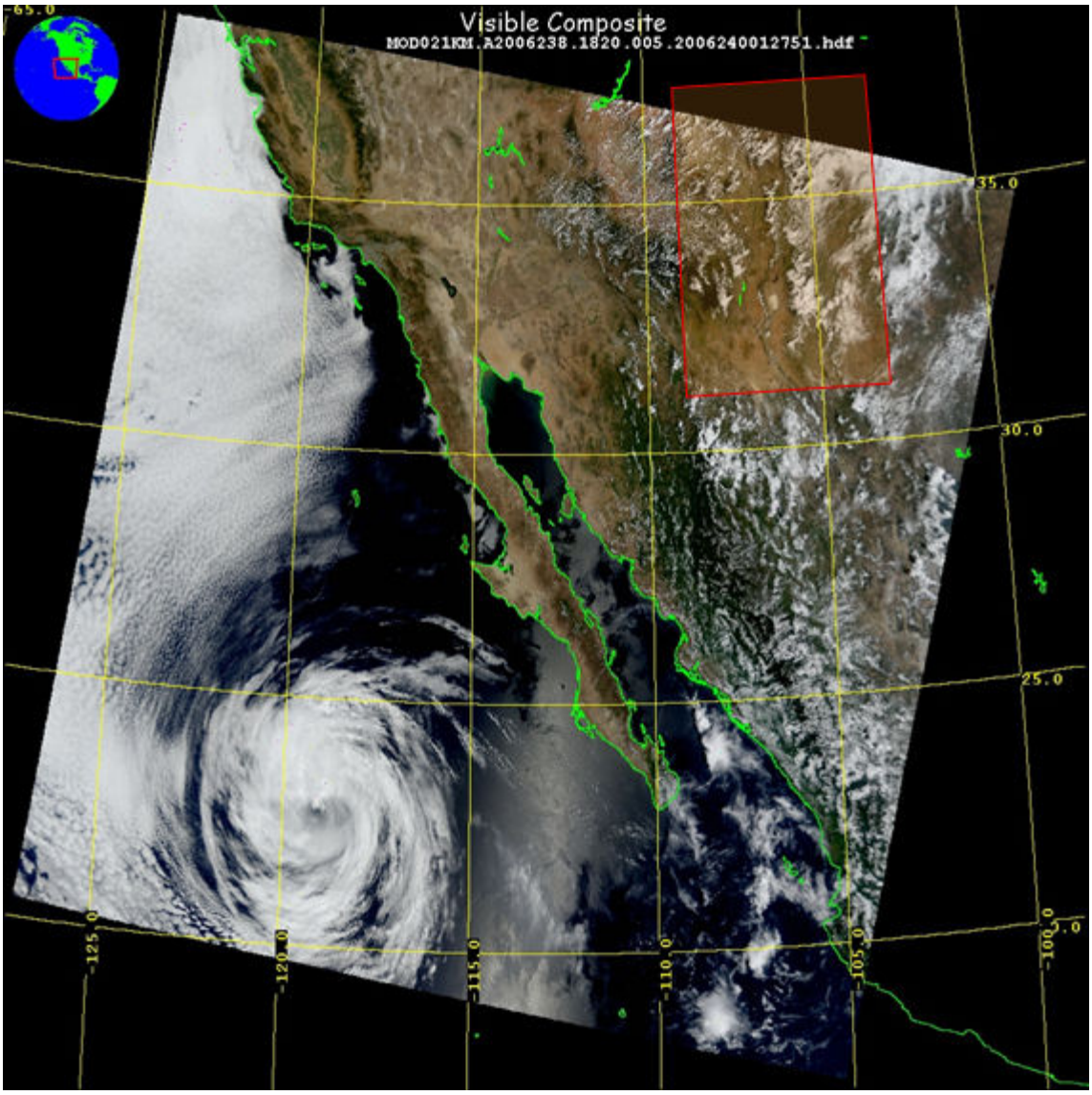

Figure 18. MODIS (Terra) true color granule image on 26 August 2006 (1820 UTC) with approximate New Mexican region superimposed

4.2 Temporal Data

The temporal history of the mean spatial cloud and clear-sky properties within the AOI are organized by stringing together the individual event statistics in chronological order. In this section, histories of selected properties are presented. In the graphical displays events are successively arranged regardless of their actual time spacing. This gives a false sense of the spacing of the 81 cloud events covering a period of 14 months, but does make the plots easier to read. Figure 19 plots the cloud coverage and total precipitation event values. Total precipitation is the summation of the 16 surface data sites daily accumulation totals situated across the state. Precipitation data was organized only from the 30 events of 2007. The left-side scale shows that the range of precipitation accumulation from those sites fell between 0 and 1.7 inches during 2007. Precipitation

totals appear somewhat periodic, especially during the JFM quarter of 2007 (before Julian day 096). From this plot it is impossible to tell if these high and low precipitation cycles occurred from consecutive day events clumped together or not. Cloud coverage measures the fraction of the AOI covered by confident cloud. This value is seen to vary from about 5 % to 100%. The correlation coefficient between these two properties during 2007 was calculated to be 0.24, indicating a very weak correlation. This is not unexpected since precipitation does not occur in all clouds and is often locally heavy. Also, the locations of the ground sites are not uniformly situated.

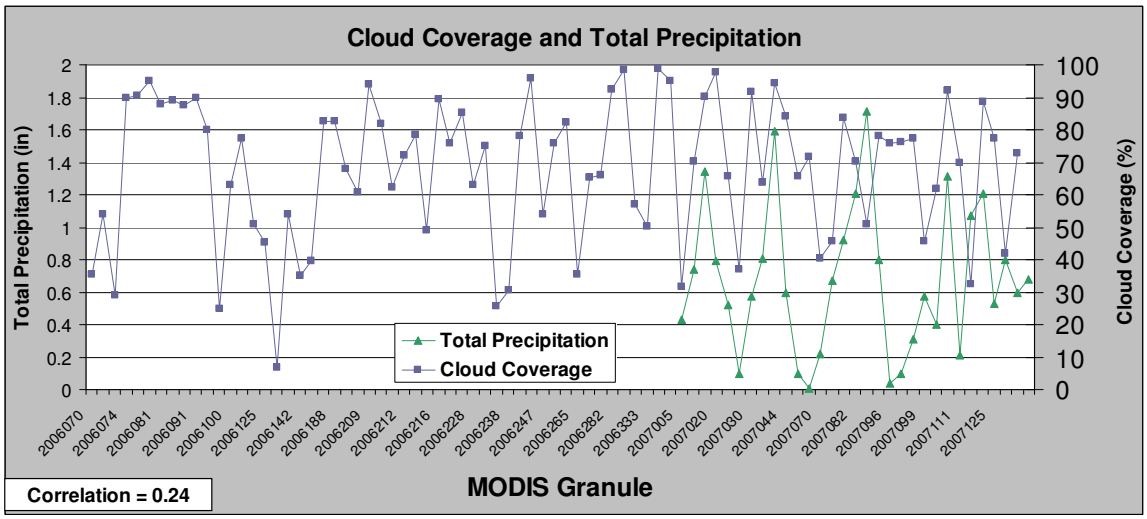

Figure 19. Mean cloud coverage and total precipitation from 81 cloudy cases over New Mexico from 11 March 2006 to 8 may 2007.

In order to evaluate the possible periodic precipitation totals, precipitation and cloud cover data from the first 100 days of 2007 is plotted in Figure 20. Lines connecting data points represent consecutive days and likely specific storm systems. It appears that a precipitation trend exists for each storm system (increasing or decreasing with time), but that no longer-term periodicity exists. The cloud cover/precipitation correlation for this period remained low. A better correlation would likely exist by comparing the hourly precipitation rate of sites covered by cloud at the time of the satellite collection.

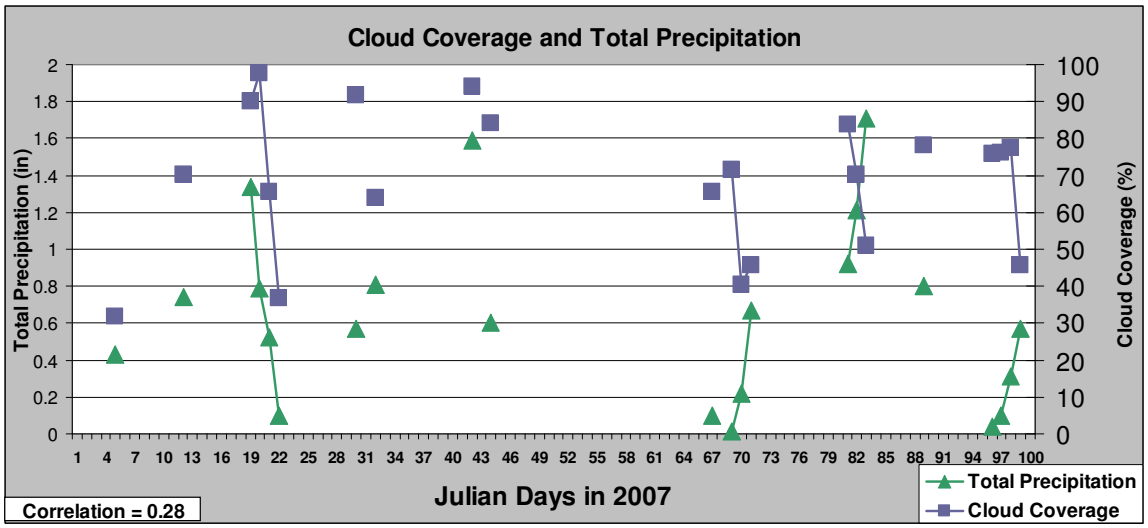

Figure 20. Same as Figure 19 except for the first 100 days in 2007.

The temporal cloud coverage percent and mean aerosol optical depth (AOD) are plotted in Figure 21. The mean clear-sky AOD values fluctuate between 0.03 and 0.4. No clear seasonal trends can be identified. There is a moderate correlation of 0.5 between AOD and cloud cover. Although this supports the indirect aerosol effect idea that increased aerosol concentrations lead to more extensive cloud fields, that conclusion cannot be drawn until a more rigorous study is performed that include cloud particle and cloud condensation nuclei (CCN) concentration estimates. Some of the data issues that may be adversely affecting these statistics are AOD retrieval errors and thin cloud contamination.

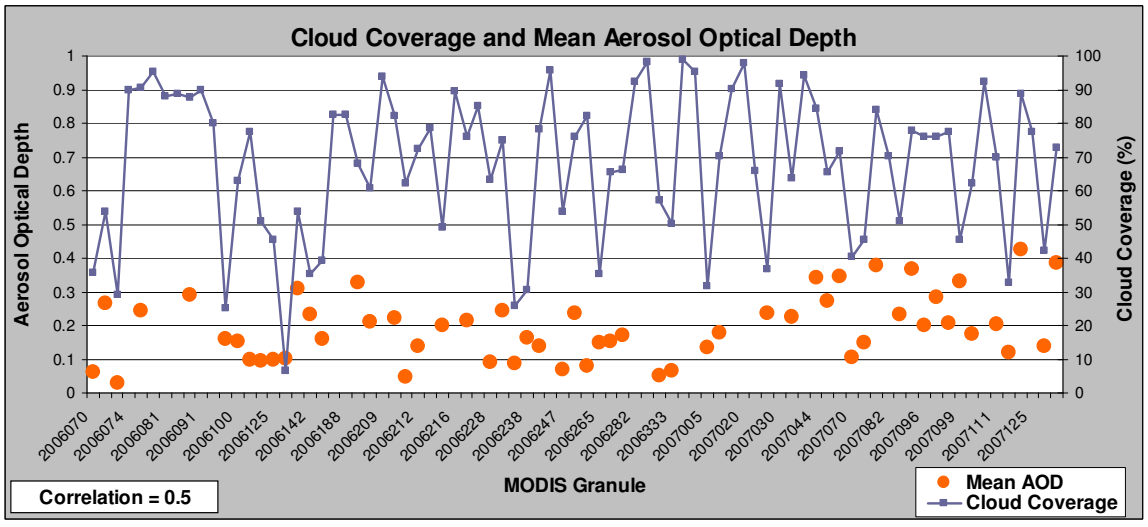

Figure 21. Same as Figure 19 except for cloud coverage and mean aerosol optical depth.

4.3 Cloud Super-Cooled Liquid Water Results

Temporal statistics of the newly derived cloud products involved in the estimation of cloud SLW are presented in this section. Figure 22 is a bar graph of the parameterized

vertical cloud thickness over the period. Disregarding the zero thickness value on day 232 of 2006, the mean event thicknesses range from 1.8 km to 5 km. The day 232 zero cloud thickness occurred because the mean cloud top temperature was 286 K, above the maximum allowable cloud SLW temperature. If this occurs then the cloud thickness is not calculated. This anomaly in the algorithm can be fixed. It is difficult to interpret these data alone since mean cloud thickness is sensitive to the number of cloud pixels and, therefore, the cloud fraction.

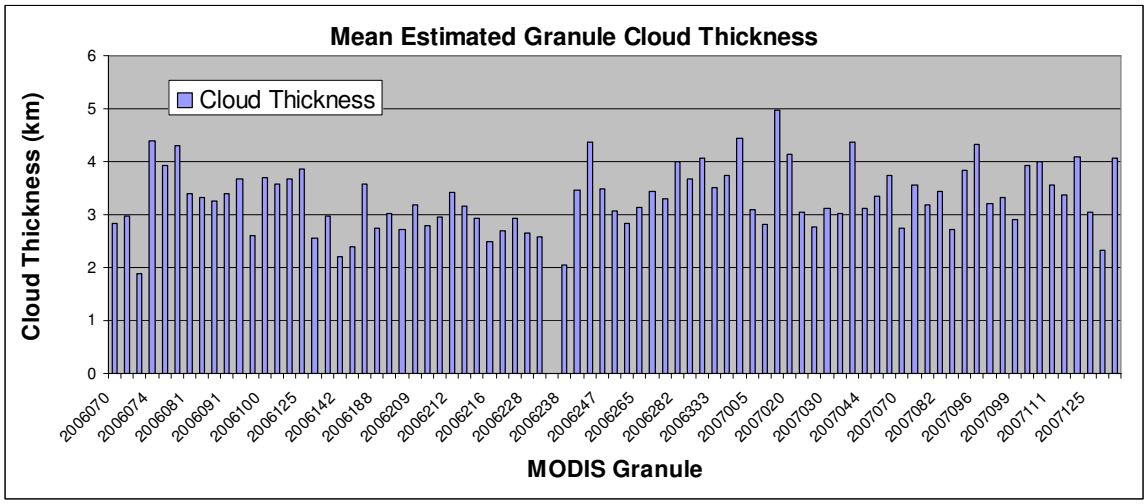

Figure 22. Same as Figure 19 except for mean estimated cloud vertical thickness.

The calculated event cloud volumes are plotted in Figure 23. Cloud volumes were derived by multiplying the area of New Mexico (315,194 km^2) by the cloud fraction (coverage) and then by the cloud estimated thickness in km. This plot gives a better feel for the amount of cloud over the state. As a result, the cloud volume data has a higher variance than the cloud thickness. The largest values are those where the cloud coverage and mean cloud thickness were high. The 129th day of 2006 had the lowest volume because the cloud fraction was 6.6% despite a moderate cloud thickness of 2.56 km.

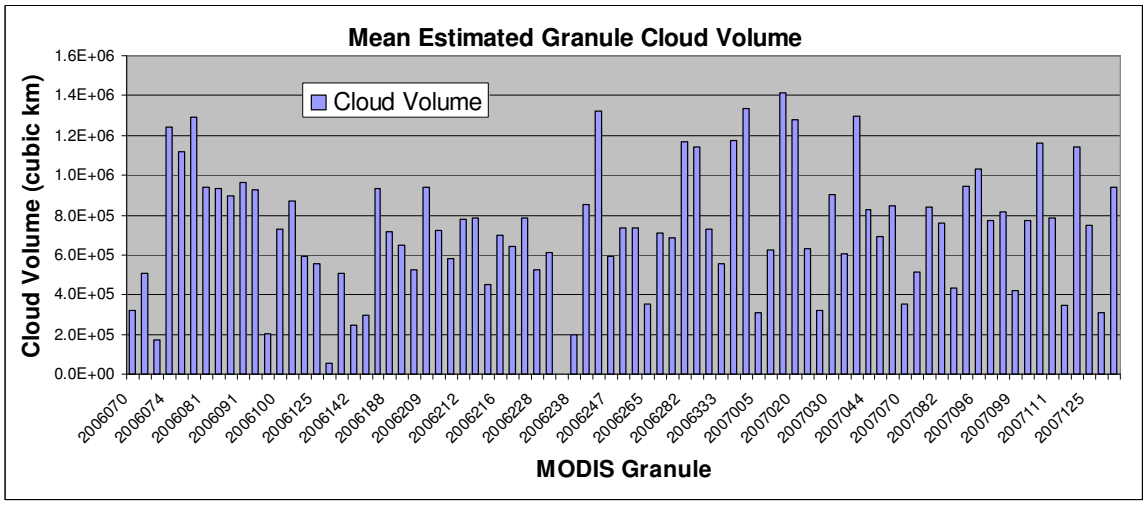

Figure 23. Same as Figure 19 except for mean estimated cloud volume.

The mean cloud SLW total mass over the AOI (blue squares) estimated for each event, along with its mean uncertainty bars (length of half the vertical bars), are plotted in Figure 24. These values are a function of the column estimated cloud SLW values and the fraction of cloud that contains a SLW layer. It may be expected that there is a seasonal dependency for cloud SLW. Although that is difficult to decipher from this dataset, the largest values of estimated cloud SLW occurred between September and March. It can also be seen that the uncertainty of the cloud SLW, taken directly from the MODIS derived cloud water path uncertainty, can be large. Since uncertainty is defined as a percent, the absolute uncertainty (plotted in units of mass) is proportional to the cloud SLW amount. Total daily precipitation accumulation is also plotted in the figure for the 2007 event days. A negligible correlation (0.17) was calculated between cloud SLW and precipitation.

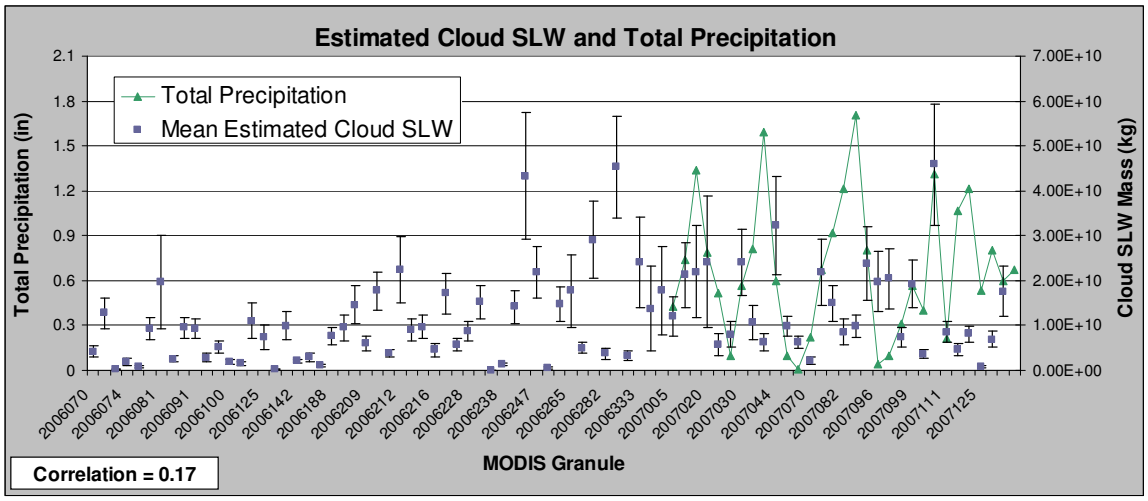

Figure 24. Same as Figure 19 except for mean estimated cloud super-cooled liquid water and precipitation accumulation (2007 only).

The correlation coefficient was calculated between the mean pixel estimated cloud SLW mass and all of the major mean cloud and clear-sky properties. These values are listed in Table 5. The cloud and clear-sky correlations are shaded in blue and orange, respectively. The correlation between total precipitation and total AOI cloud SLW mass (as opposed to mean pixel mass), already mentioned, is listed on the last line of the table. The cloud coverage was also correlated to total AOI cloud SLW mass since both of these quantities are total AOI statistics. The mean pixel statistics are correlated to the mean pixel cloud SLW mass. None of the clear-sky properties appear correlated to cloud SLW in any degree. Cloud effective emissivity and effective particle radius also show little correlation. The rest of the cloud properties show some correlation to cloud SLW estimates. Interestingly, cloud top temperature (CTT) and cloud thickness possess low correlation coefficients. Cloud SLW is maximized if the cloud top temperature is near 250 K, which is about an average value for this property. By both increasing and decreasing the CTT, the amount of cloud SLW decreases causing a low correlation. The correlation between mean cloud SLW and the absolute value of the CTT and 246 K difference provided the highest correlation with CTT at -0.61. As temperature gets

farther from the 246 K value, the mean cloud SLW decreases. Since cloud thickness increase with decreasing temperature and low CTT become farther from 246 K, large cloud thicknesses do not necessarily result in high cloud SLW amounts. The mean cloud properties with the highest correlation with mean cloud SLW are the cloud optical depth (COD) and cloud water path (CWP). These two cloud properties are themselves highly correlated, so it is not surprising that they both generate high correlation with mean cloud SLW. The calculation of cloud SLW is made by taking the calculated SLW fraction of the MODIS derived CWP, therefore CWP is highly proportional to estimated cloud SLW. In the end, the more water the cloud possesses, the higher the probability that some of that will be in the super-cooled phase.

Table 5. Summary of estimated cloud SLW correlation with other derived values.

Correlation	Correlation to Mean Cloud SLW
Cloud Coverage	0.34*
Mean Cloud Top Temperature	0.25
Mean Cloud Top Pressure	0.22
Mean Cloud Effective Emissivity	0.02
Mean Cloud Optical Depth	0.73
Mean Cloud Effective Particle Radius	0.05
Mean Cloud Water Path	0.78
Mean Cloud Thickness	0.22
Mean Cloud Liquid Water (CLW)	0.40
Mean SLW Fraction	0.42
Mean Cloud SLW Uncertainty	0.53
Mean Aerosol Optical Depth	-0.05
Mean Angstrom Exponent	-0.12
Mean Column WV NIR	-0.17
Mean Column WV IR	-0.12
Mean Lifted Index	0.02
Total_Precipitation	0.17*

*correlation with total AOI cloud SLW mass

4.4 Regional Analysis

The CSEA code was run using the same data, but with a much smaller AOI. The focus was on a 1° x 1° region in northern New Mexico with boundaries from 36° N to 37° N and from 105° W to 106° W. This AOI is superimposed on the map of the northern half of New Mexico in Figure 25. It includes the northern part of the Sangre de Christo Mountains in New Mexico and contains the three ground sites of Chama, Taos airport, and Red River Pass. This area was chosen because it was suspected to experience substantial cloud cover and rainfall.

Figure 25. Location of 1º x 1º AOI region centered over Taos, NM.

The AOI mean cloud thickness in this region is plotted in Figure 26. The variation in cloud thickness values are greater than the mean thickness for the entire New Mexico AOI shown in Figure 22. This is likely due to the fact that extreme values influence the mean value more so in a smaller set of data. There are many days where no cloud was observed over the region. At the same time, the range of cloud thickness values (1.6 km – 5.3 km) is similar to that of the large New Mexico AOI due to the limits of the parameterization scheme employed.

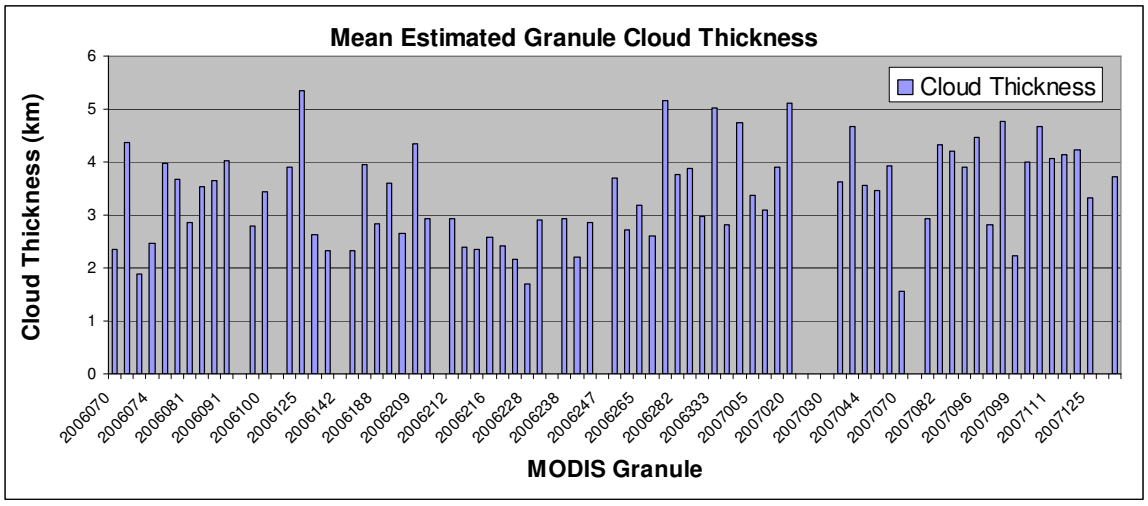

Figure 26. Same as Figure 19 except for 1º x 1º region centered over Taos, NM.

The estimated AOI cloud SLW mass and total precipitation (2007 events only) are plotted in Figure 27 as was done previously for the entire state AOI. Large cloud SLW events appeared to take place in the last quarter of 2006, then again in the spring of 2007. The correlation of estimated cloud SLW and precipitation from the three ground sites contained in the smaller AOI was moderately high at 0.66. This is much larger than the previous SLW-precipitation correlation for the entire state. This was likely caused by the focus on a region close to the ground sites where precipitation is measured.

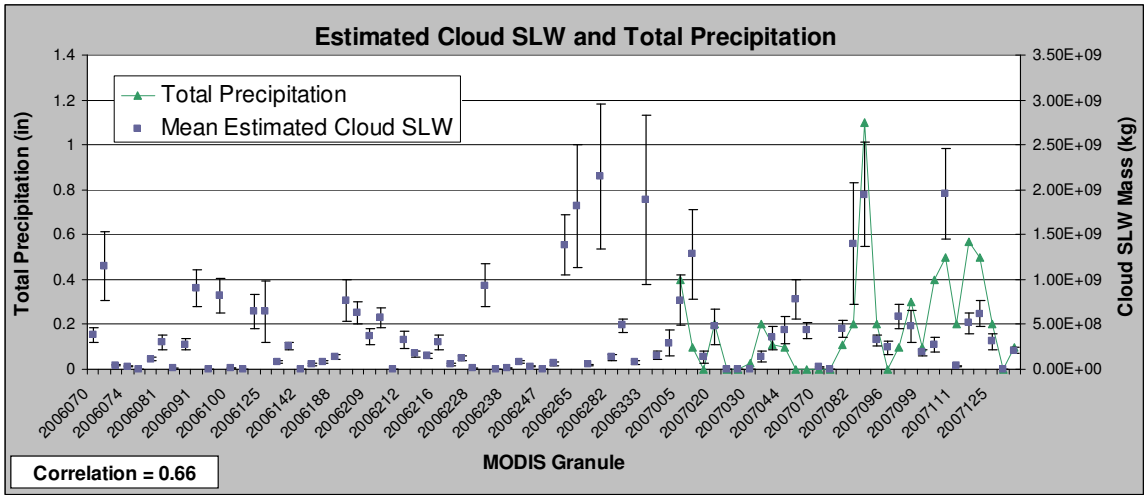

Figure 27. Same as Figure 26 except for 1º x 1º region centered over Taos, NM.

4.5 Sensitivity

The estimation of cloud SLW is based on many assumptions, parameterizations, and conditioning thresholds. In order to understand the potential errors and quantify the uncertainty in the derived values, several sensitivity tests have been performed. Six important cloud properties are derived in the process of estimating the cloud SLW. These properties include cloud thickness, cloud liquid water mass, cloud SLW fraction, cloud SLW, cloud water path uncertainty, and cloud coverage. The results of these six properties were recorded as single algorithm parameters were altered in order to understand their responses. A final result was produced for each property. For cloud thickness, cloud SLW fraction, and cloud water path uncertainty the final result was the temporal mean of the all of the event spatial means. For the other three cloud properties, the result was a temporal mean of the event total quantity such as fractional cloud cover, total cloud liquid water mass and SLW mass.

The *COD_min_thres* variable lets the user determine which cloud pixels will be analyzed for SLW by setting a minimum cloud optical thickness given by the MODIS derived COD. Changing this variable will change the number of pixels examined and therefore directly change cloud coverage percent. Indirectly it will likely change the set of cloudy pixels by either increasing or decreasing the number of thin cloud pixels. Two algorithm runs were performed with the *COD_min_thres* variable set to 5 and then to 1 and the results are displayed in Table 6. The last column gives the percent change of lowering the threshold from 5 to 1, and likely increasing the number of thin clouds in the cloud pixel dataset. As expected the cloud coverage increased with more thin cloud, but for the average event the increase was less than 1%. The mean spatial cloud thickness estimate decreased by just over 5%. The fraction of the cloud containing SLW did not change very much, yet the average event cloud SLW mass did increase by nearly 23%. This seems like an inconsistency, but these metrics do not correlate well since the mean cloud SLW fraction is a spatial mean, while the cloud SLW mass is a total scene result. The

increased number of cloudy pixels examined does increase the total cloud SLW of the scene, but does not increase the *mean* pixel fraction of cloud SLW. This is also reflected in the average event *total scene* cloud liquid water mass, as it increased by nearly the same amount as the total cloud SLW mass. The mean CWP uncertainty increased by about 4% indicating that there is greater uncertainty in derived cloud water in thinner clouds. The interesting result of this is that this small addition (0.54 percent) to the total cloud coverage increased the total cloud SLW mass by such as large amount. The minimum COD threshold used in the standard runs is set to 1. This was done due to the large percent of cloud SLW contained in clouds with COD values between 1 and 5.

Table 6. Summary of mean derived cloud properties as a function of minimum COD.

Cloud Parameter	COD > 5	COD > 1	Change (%)
Cloud Coverage (%)	67.8	68.2	0.54
Mean Cloud Thickness (km)	3.4	3.2	-5.62
Cloud Liquid Water Mass (kg)	2.43E+10	3.03E+10	24.98
Cloud SLW Mass (kg)	1.19E+10	1.46E+10	22.77
Mean Cloud SLW Fraction (%)	53.1	53.2	0.16
Mean Cloud Water Path Uncertainty (%)	31.4	32.7	4.32

The second sensitivity test performed varied the *CloudThickMax* variable which is responsible for limiting the parameterized cloud thickness to a certain value. Four algorithm runs were made with this variable set to 2 km, 4 km, 6 km, and 20 km. The results are given in Table 7, with the 20 km results listed first and the percent change for the other runs calculated with respect to this 20 km run. Cloud coverage is not affected by the maximum cloud thickness and does not change from run to run. Total cloud liquid water does not change either. The cloud liquid water is derived by spatially integrating the column cloud liquid water path (CWP), and is, therefore, only a function of the number of cloudy pixels in the scene. The mean event cloud thickness, of course, is directly affected and decreases with lower minimum settings. Clouds were about 42% thinner on average using the low 2 km minimum than when utilizing the nearly unlimited thickness condition. When looking at the mean event cloud thickness values in the bar graphs previously presented one can see that nearly every event possessed a mean cloud thickness above 2 km, but very few events possessed means greater than 4 km or 6 km. The mean cloud thickness decreased by only about 1 % when restricting the cloud thickness to 6 km. This restriction resulted in very little change in any cloud property. The parameterization method for cloud thickness only produces values greater than 6 km for very cold clouds with very high COD values. The estimated cloud SLW mass did suffer a 27 % and 11 % reduction when the cloud thickness was limited to 2 km and 4 km, respectively. This result was due to thinner clouds, and a reduction in the overall fraction of the cloud possessing SLW, and not due to reduced cloud liquid water content. The main result is that thinner clouds have a lower probability of containing a layer of SLW.

Table 7. Same as Table 6 except for maximum cloud thickness.

Cloud Parameter	CldThk < 20 km	
Cloud Coverage (%)	68.2	
Mean Cloud Thickness (km)	3.2	
Cloud Liquid Water Mass (kg)	3.03E+10	
Cloud SLW Mass (kg)	1.46E+10	
Mean Cloud SLW Fraction (%)	53.2	
Mean Cloud Water Path Uncertainty (%)	32.7	
Cloud Parameter	**CldThk < 2 km**	**Change (%)**
Cloud Coverage (%)	68.2	0.00
Mean Cloud Thickness (km)	1.9	-41.51
Cloud Liquid Water Mass (kg)	3.03E+10	0.00
Cloud SLW Mass (kg)	1.06E+10	-27.05
Mean Cloud SLW Fraction (%)	46.5	-12.48
Mean Cloud Water Path Uncertainty (%)	32.7	0.00
Cloud Parameter	**CldThk < 4 km**	**Change (%)**
Cloud Coverage (%)	68.2	0.00
Mean Cloud Thickness (km)	2.9	-8.69
Cloud Liquid Water Mass (kg)	3.03E+10	0.00
Cloud SLW Mass (kg)	1.30E+10	-10.76
Mean Cloud SLW Fraction (%)	51.4	-3.29
Mean Cloud Water Path Uncertainty (%)	32.7	0.00
Cloud Parameter	**CldThk < 6 km**	**Change (%)**
Cloud Coverage (%)	68.2	0.00
Mean Cloud Thickness (km)	3.1	-1.29
Cloud Liquid Water Mass (kg)	3.03E+10	0.00
Cloud SLW Mass (kg)	1.46E+10	-0.18
Mean Cloud SLW Fraction (%)	53.2	-0.02
Mean Cloud Water Path Uncertainty (%)	32.7	0.00

By varying *MoistAdiabaticLapaseRate* variable, one can change the rate at which the estimated cloud temperature increases with decreasing altitude. This can have a pronounced affect on the cloud temperature range and therefore on whether or not there exists a SLW layer. This moist adiabatic lapse rate (MALR) in saturated environments is considered to be close to 6 K/km, but can decrease dramatically with high water vapor content. Therefore, two algorithm runs were made using a MALR value of 6 K/km and 2 K/km. The individual run results and the resulting percent change, from decreasing the MALR from 6 to 2, are given in Table 8. The only two properties affected by this variable are the mean estimated cloud SLW fraction and the total cloud SLW mass. A nearly 30 % reduction in cloud SLW mass per event resulted by decreasing the MALR. Again, this resulted by decreasing the cloud temperature range and reducing the chances that a SLW temperature layer exists in the cloud.

Table 8. Same as Table 6 except for moist adiabatic lapse rate.

Cloud Parameter	MALR = 6 K/km	MALR = 2 K/km	Change (%)
Cloud Coverage (%)	68.2	68.2	0.00
Mean Cloud Thickness (km)	3.2	3.2	0.00
Cloud Liquid Water Mass (kg)	3.03E+10	3.03E+10	0.00
Cloud SLW Mass (kg)	1.46E+10	1.03E+10	-29.31
Mean Cloud SLW Fraction (%)	53.2	45.7	-14.02
Mean Cloud Water Path Uncertainty (%)	32.7	32.7	0.00

The cloud liquid water fraction parameterization will produce SLW fractions at every cloud temperature, albeit at low percentages for very low temperatures. The *SCLW_min_thres* variable limits the estimation of cloud SLW at a certain minimum temperature value. This gives the user more control on where the SLW is defined in the cloud. Four algorithm runs were performed with the minimum allowable temperature for SLW set at 200 K, 233 K, 243 K, and 253 K. The 200 K value, in essence, lets the parameterization of cloud SLW liquid water determine the amount of SLW since a nearly zero SLW percent is calculated at that temperature or below. All subsequent runs with higher minimum temperatures are compared to the 200 K run and the percent change in the properties is noted. The results of these algorithm runs are presented in Table 9. Only the mean cloud SLW fraction and the total cloud SLW mass are reported in the table since these are the only cloud properties that are sensitive to this variable. Very little change is seen in total cloud SLW mass when the minimum temperature is set as high as 243 K. This means that most of the parameterized cloud SLW exists above this temperature. Cloud SLW mass reduces by nearly one-quarter when the minimum allowable temperature is set to 253 K (-20º C).

Table 9. Same as Table 6 except for minimum SLW temperature threshold.

Cloud Parameter	SLW Min = 200 K	
Cloud SLW Mass (kg)	1.46E+10	
Mean Cloud SLW Fraction (%)	53.2	
Cloud Parameter	**SLW Min = 233 K**	**Change (%)**
Cloud SLW Mass (kg)	1.46E+10	-0.25
Mean Cloud SLW Fraction (%)	53.3	0.31
Cloud Parameter	**SLW Min = 243 K**	**Change (%)**
Cloud SLW Mass (kg)	1.41E+10	-3.58
Mean Cloud SLW Fraction (%)	53.0	-0.37
Cloud Parameter	**SLW Min = 253 K**	**Change (%)**
Cloud SLW Mass (kg)	1.10E+10	-24.52
Mean Cloud SLW Fraction (%)	48.6	-8.53

The theoretical sensitivity of the estimated cloud SLW mass due to the fractional liquid water parameterization was made by analytically assessing the equation used for the parameterization when the defined constants were altered. The temperature offset constant, a_2, from equation (2) affects the horizontal position (temperature) of the cloud liquid fraction curve. The temperature that produces a 0.5 cloud liquid water fraction is a good point of reference because the curve is symmetrical about this point. Using the

predefined value of -25, this symmetry point was positioned at 250 K. Figure 28 shows the plots of the three cloud liquid fraction curves with a_2 values of -24, -25, and -26. The symmetry points for the curves with a_2 values of -24 and -25 are at 240 K and 260 K, respectively. Integrating under the curves gives an area representing the total cloud SLW content. Integration of each curve was performed between temperatures of 220 K to 280 K. An increase (decrease) in cloud SLW content of 33.04 % was found when changing the a_2 variable to -24 (-26). A potential 3.3 % increase in cloud SLW content results for an increase of +1 to the a_2 variable (a decrease in the symmetry point of the curve by -1 K).

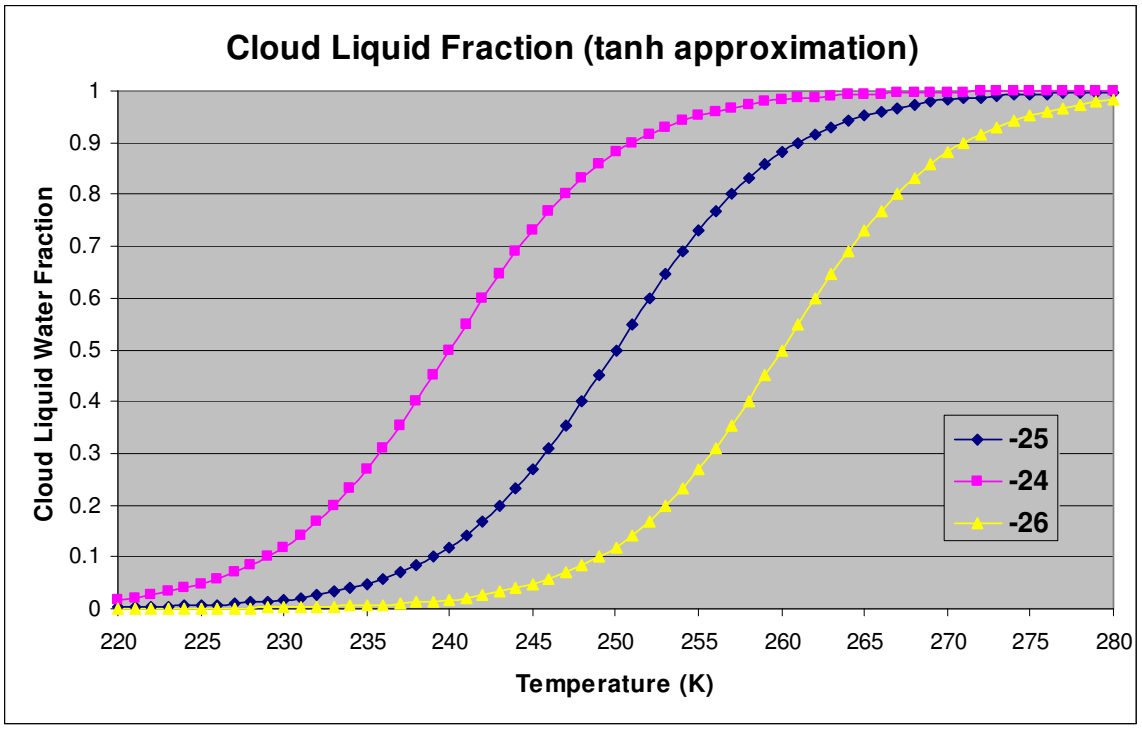

Figure 28. Cloud liquid fraction parameterization using three values of a temperature offset.

5. VALIDATION

Validation of the CSEA code does not include direct comparisons of the estimated cloud super-cooled liquid water, but, rather, comparisons of some of the derived products used in its calculation. Thus far, the derived MODIS and CSEA code products have been compared to vertical profiles of derived cloud products from the CloudSat space-based radar. This comparison has been performed for only one event as a proof of concept. This section will describe this cloud product comparison process in detail. All of the MODIS data obtained for the temporal study was collected by the sensor onboard the Terra satellite because its overpass time coincided very closely with the GOES imagery that was used to determine the cloudy events. Comparisons of CloudSat and MODIS/Terra data would be very difficult due to the roughly two-hour latency between the collections. On the other hand, the CloudSat satellite collects data just after, and in the same FOV, as the MODIS sensor onboard the Aqua satellite as they are both part of the satellite group situated on the same orbit called the "A-Train". A cartoon, taken from the NASA webpage, of the satellites comprising the "A-Train" constellation is shown in Figure 29. Based on the local overpass times given next to each satellite in the image, it can be seen that the CloudSat satellite follows the AQUA platform by about one minute.

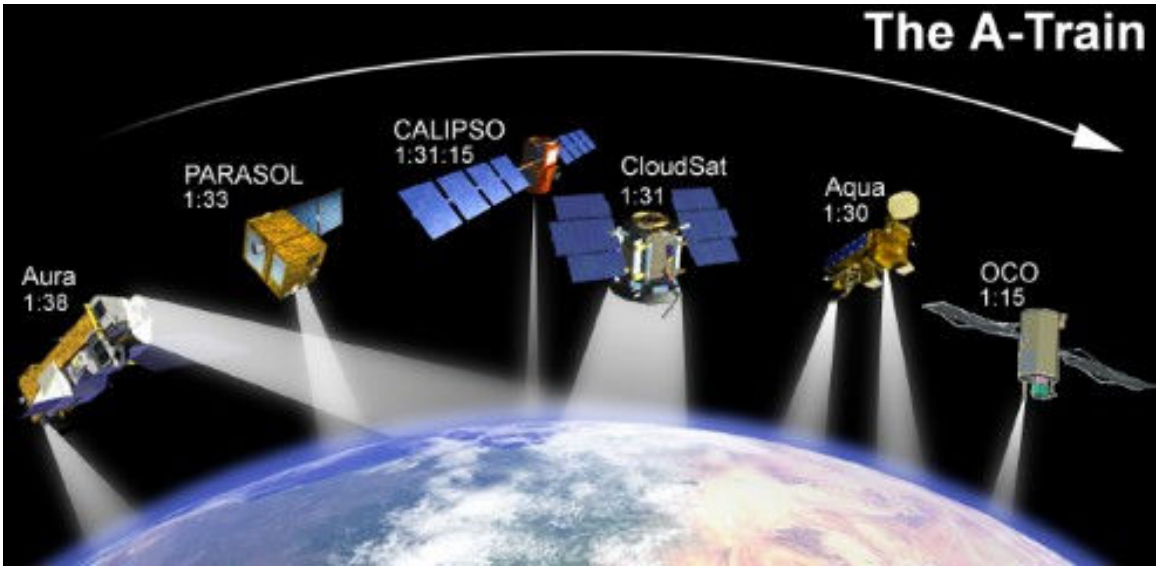

Figure 29. NASA depiction of the satellites that make up the "A-Train" constellation.

MODIS data from the AQUA satellite and CloudSat data were obtained on 24 March 2007 at the MODIS granule time of 1945 GMT. The true-color image made in rectangular MODIS sensor space using MODIS bands 1, 4, and 3 for the colors red, green, and blue (RGB), respectively, is shown in Figure 30. The red polygon identifies the boundaries of the AOI defined between the latitudes of 35º N and 45º N, and longitudes 90º W to 110º W. This region is centered over the mid-section of the United States. This dataset was chosen because of the presence of large-area cloud cover. It contains the majority of a mature mid-latitude cyclone with widespread cloud cover arching across the scene along a warm front and wrapping around the center low

pressure. The slightly narrower cloud field vertical aligned in the image likely corresponds to an occluded/cold front. The yellow dashed line shows the position of the CloudSat FOV as it cuts through the MODIS granule. Along most of the CloudSat FOV path clouds are present, but there are also patches of clear-sky.

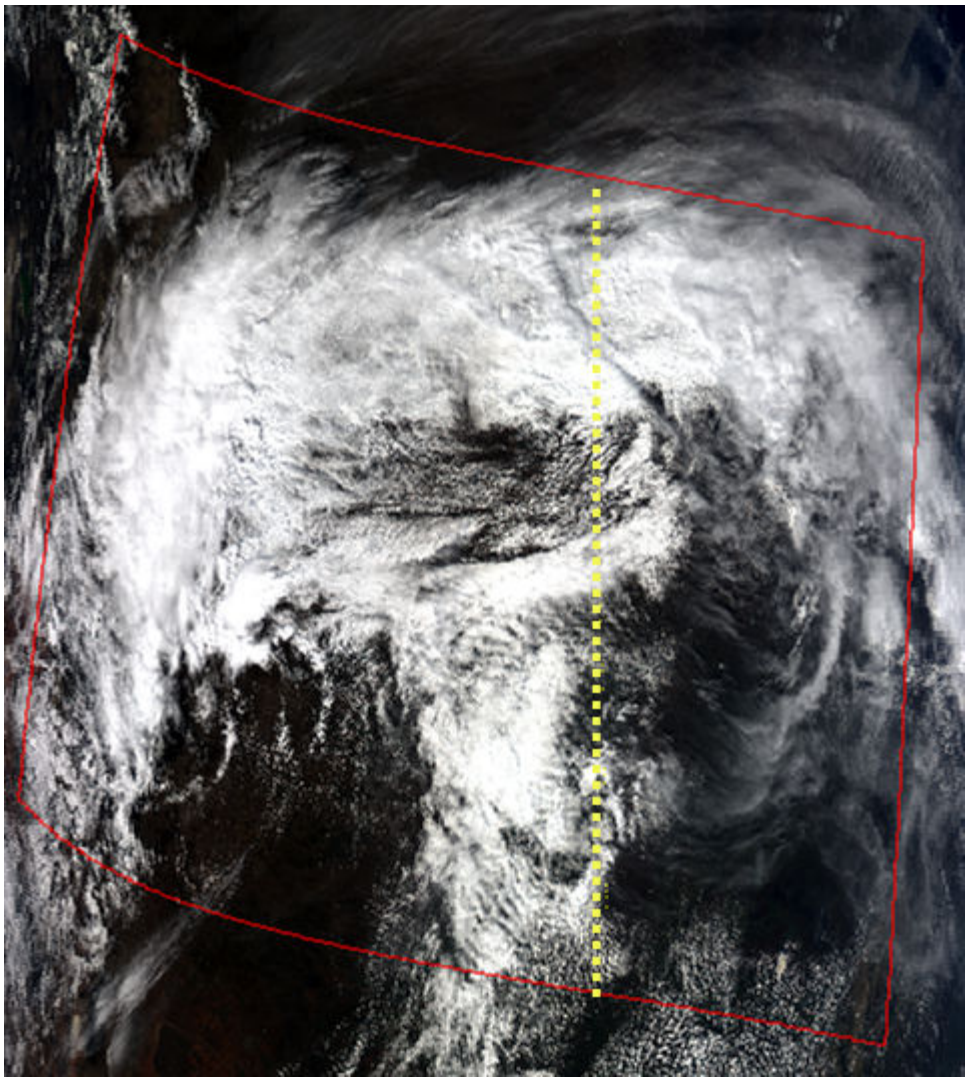

Figure 30. CLOUDSAT observing path (dashed yellow line) across the MODIS (Aqua) true color image with highlighted area of interest (red boundaries) for the 24 March 2007 MODIS granule.

The CloudSat vertical cloud mask profile is displayed above the CloudSat horizontal path (yellow dashed line) across the MODIS imagery in Figure 31. CloudSat detected clouds correspond well to the MODIS cloud fields as one would expect. The thick clouds with increasing tops in the leftmost (northern) portion of the profile are associated with rising moist air over the warm front. Both high cirrus and low water clouds appear intermittently in the middle of the profile. In the right half of the profile, tall cumulonimbus clouds are seen that were likely produced by the approaching cold front.

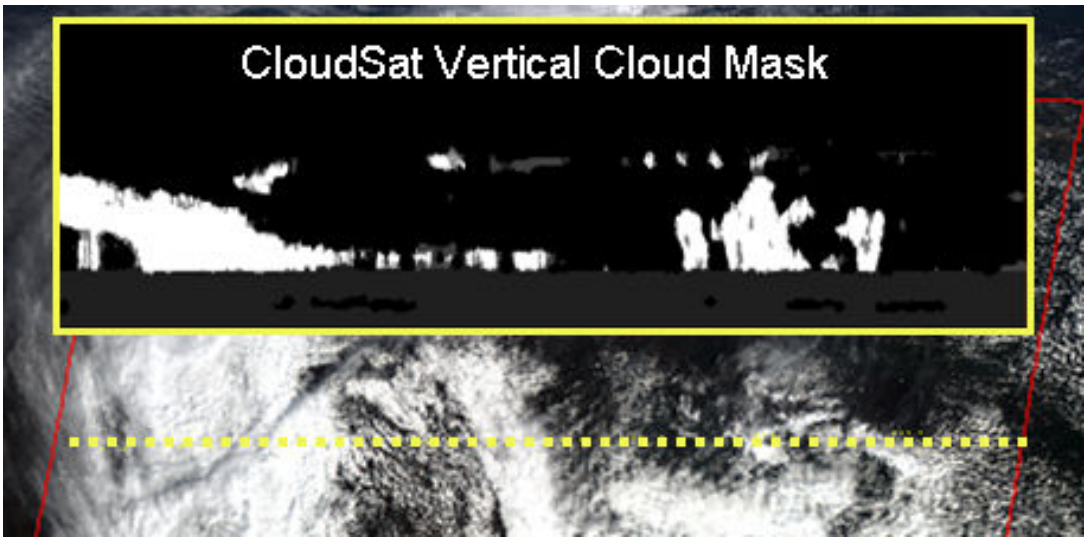

Figure 31. CLOUDSAT vertical reflectivity Quicklook along side approximate corresponding MODIS (Aqua) true color image in the 24 March 2007 MODIS granule.

The first step in comparing Cloudsat cloud products to those of MODIS and the CSEA code is to accurately identify the corresponding data pixels. CloudSat data pixels have roughly a 1.4 km by 1.7 km horizontal size. Since this data will be compared to the MODIS 5 km horizontal resolution data, CloudSat data pixels are matched to MODIS data pixels. This is done by simply determining if individual CloudSat pixels lie within the defined AOI and then identifying the closest MODIS pixel using the associated geo-location information. The final product is shown in Figure 32 as the CloudSat pixel mask (white) superimposed on the AOI mask (gray) in MODIS granule space.

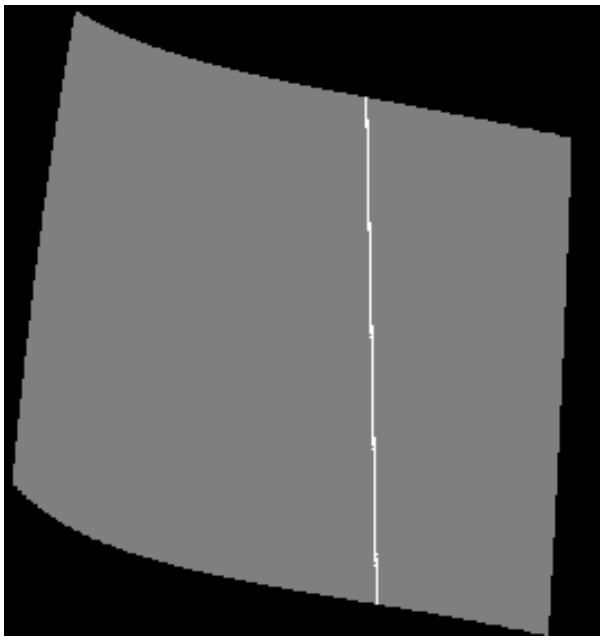

Figure 32. Derived locations of the AOI (Gray) and CloudSat FOV path (White) in the 24 March 2007 MODIS granule.

For each MODIS 5 km pixel, the derived MODIS/CSEA cloud properties were compared to the mean CloudSat derived cloud properties from all of the CloudSat pixels that were matched with the MODIS pixel. Differences between the MODIS/CSEA and CloudSat properties were calculated and stored only when retrieved data (non-zero or fill value) from both sensors existed. In this case study, 1045 CloudSat pixels were contained inside the defined AOI. These pixels were matched with a total of 249 MODIS pixels for a ratio of about 4.2 CloudSat pixels per MODIS pixel. The mean differences between the four MODIS/CSEA and CloudSat derived cloud properties for this case are listed to three significant figures in Table 10. All of the differences have negative values meaning that the MODIS/CSEA derivations are smaller than the CloudSat properties on average. MODIS underestimates the cloud top height by only about 70 m. This is not unexpected since the cloud emissivity is not 1 and therefore radiation from below the actual cloud top is collected by the sensor, which imparts a lower altitude bias. The CloudSat cloud mask vertical resolution is about 240 m. The small cloud top height difference lies within this vertical bin distance. The difference between the other cloud properties is more dramatic and will be discussed in more depth.

Table 10. List of the mean cloud property difference between MODIS/CSEA and CloudSat.

Derived Cloud Property	MODIS/CSEA – CloudSat Difference
Mean Cloud Top Height	-0.067 km
Mean Cloud Thickness	-2.11 km
Mean Cloud Optical Depth	-1.88
Mean Cloud Liquid Water Path	-415 g/m^2

The MODIS/CSEA and CloudSat cloud top and cloud base heights are plotted with respect to latitude in Figure 33. The latitude scale is linear with higher latitudes (northern) to the left and mimics the nearly north-south CloudSat path across the scene. Data from adjacent pixels are connected by lines, while non-adjacent data points are not. The CloudSat cloud top heights are nearly always greater than the MODIS/CSEA heights. Some exceptions where MODIS CSEA cloud tops are higher than the CloudSat heights do exist for a short distance. This is likely due to the calculation of 25 km^2 cloud top height from the MODIS pixel aggregation process. CloudSat 1.7 km x 1.4 km pixels can better spatially resolve the actual cloud top heights. Around 42.5º N the MODIS/CSEA cloud base dips below sea level and the surface height shown as green lines in the clear-sky regions. This is an artifact of the cloud thickness parameterization, and can perhaps be fixed by utilizing the MODIS surface elevation product. There appears to be a limit to the CloudSat cloud base height at about 1.6 km. Whether or not this occurs due to the actual cloud base or to sensor noise near the surface and boundary layer is unknown. The CloudSat cloud thicknesses are a little more than 2 km thicker than calculated by MODIS/CSEA. This is apparent in Figure 33 as CloudSat cloud top and base heights seem to be mainly higher and lower than the corresponding MODIS/CSEA heights, respectively. Much of this is real, but some of this apparent cloud thickness is due to multilayer clouds being thought of as vertically continuous. The vertical CloudSat cloud mask is plotted in Figure 34 using the same linear latitude scale. Multilayer clouds causing an overestimation of CloudSat cloud thickness can be seen between 42.5º N - 43º

N and between 40º N - 41º N. This inaccuracy can be fixed with a more sophisticated examination of the CloudSat cloud mask.

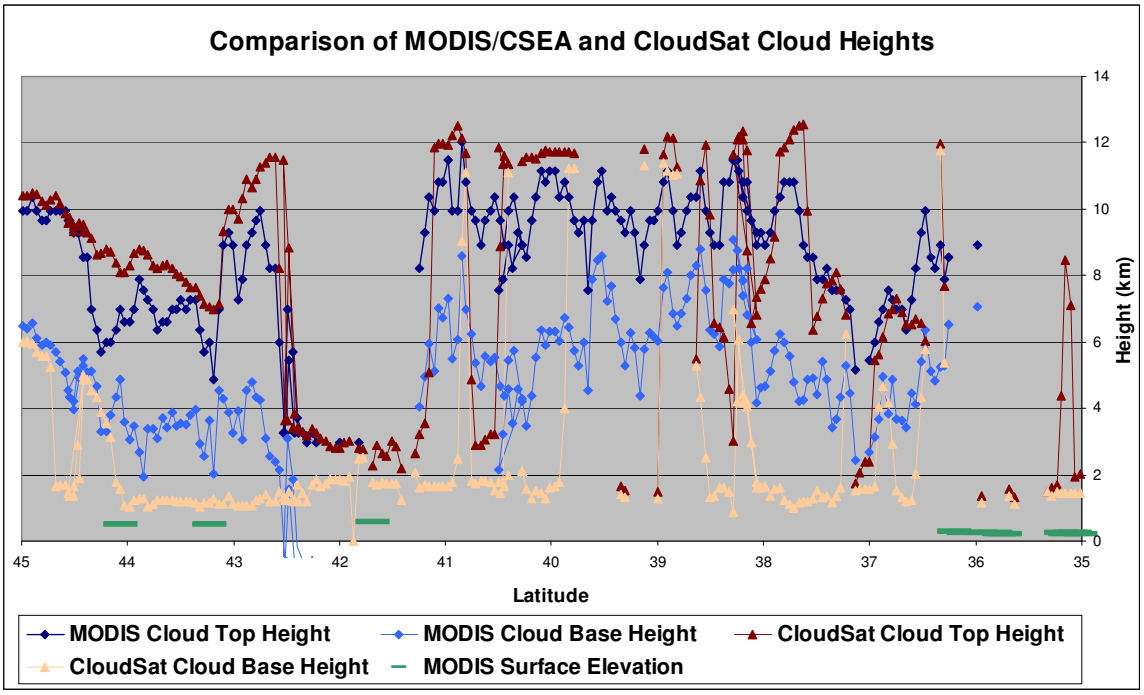

Figure 33. MODIS/CSEA and CloudSat cloud top and base heights plotted versus latitude for the case study.

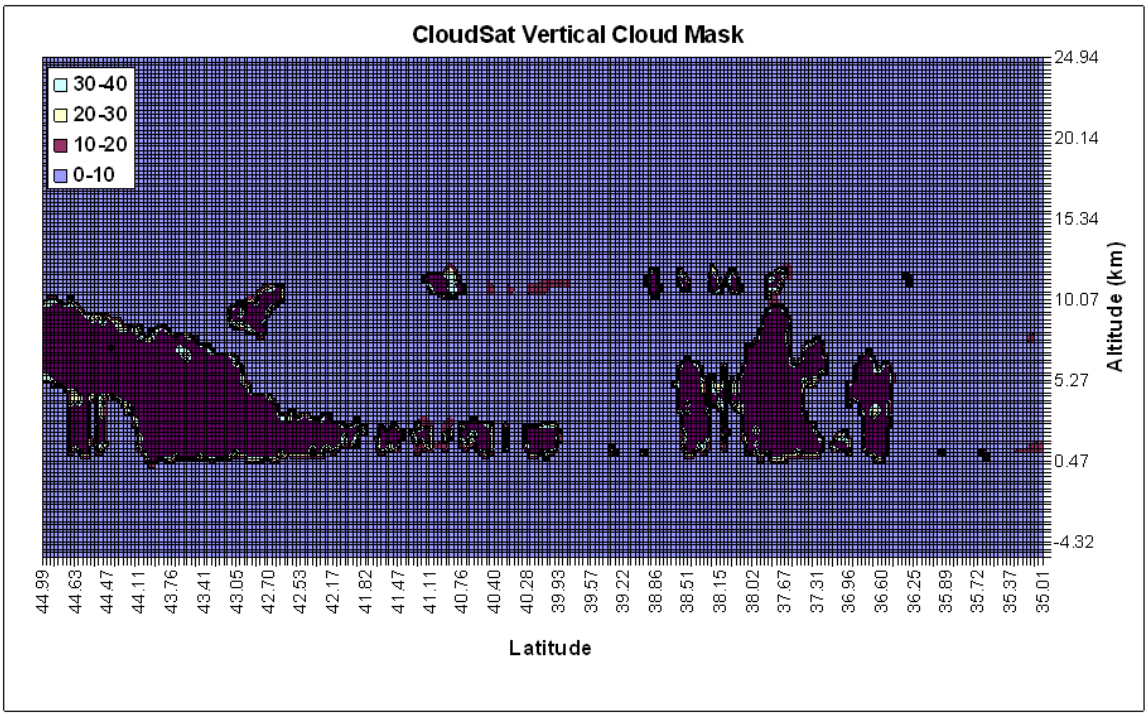

Figure 34. Same as Figure 33 except only for the CloudSat vertical cloud mask.

The CloudSat derived column optical depths are on average about 2 higher than the derived MODIS COD averaged at 5 km resolution. This difference is insignificant if the COD is large, but not so for optically thin clouds. Figure 35 shows the mean CloudSat and 5 km averaged MODIS COD values plotted against latitude for this case study in the AOI. The agreement between the two curves is fairly good even for COD values below 10. A limit of 100 was imposed upon the CloudSat values since this is the maximum allowable value for MODIS COD. There is a great deal of CloudSat COD data points that do not have corresponding MODIS COD values (between 41.5º N – 42.5º N and 35º N – 36.2º N). The CloudSat COD values show that these clouds are optically thick. The reason for the missing MODIS COD values is due to the fact that these clouds are warm (see the corresponding low cloud top heights in Figure 33) and no cloud thickness values were calculated as a result. Only clouds containing SLW were assessed in this validation procedure. These unmatched CloudSat data did not contribute to the statistical comparisons.

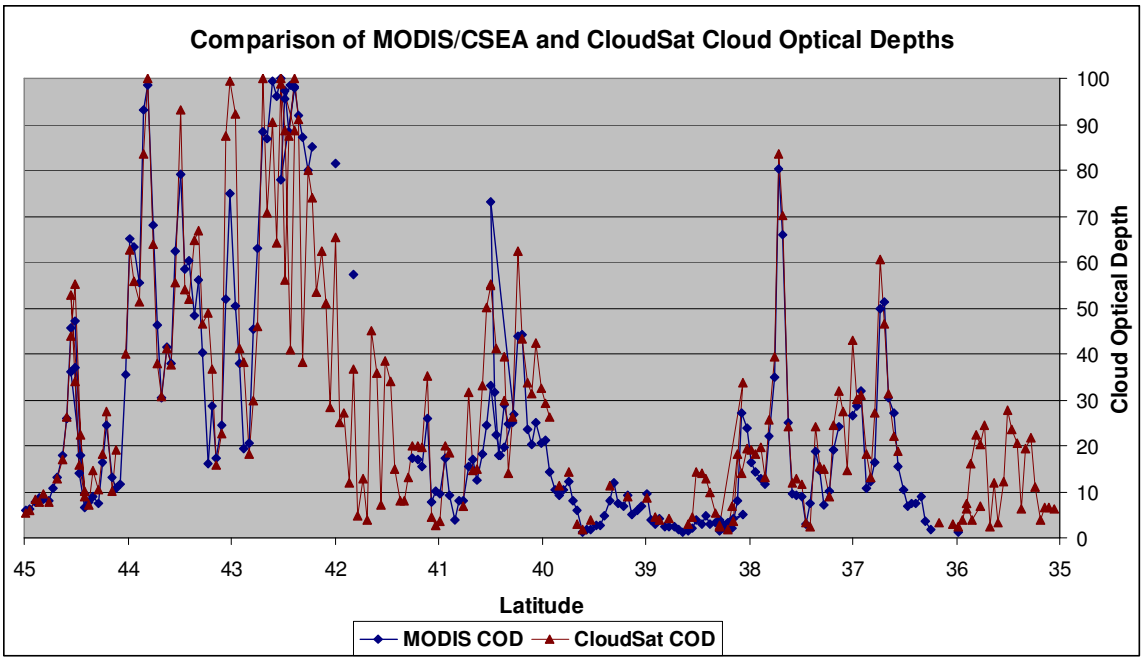

Figure 35. Same as Figure 33 except for cloud optical depth.

The largest difference between the CloudSat and MODIS/CSEA derived cloud products is in the cloud liquid water path. CloudSat derived an average of just over 400 g/m^2 more cloud column liquid water than MODIS, which represents about 150% of the mean MODIS value of 276 g/m^2. The CloudSat and MODIS cloud liquid water path values are plotted in Figure 36. Comparisons are good for high cloud (44º N – 45º N and 40.5º N – 41.2º N) where the amount of liquid water is small, but quite different for vertically thick clouds. MODIS can not capture the total cloud liquid content for clouds that are vertically and optically thick. By measuring radiation passively, information well below the cloud top cannot be obtained unlike radar that can retrieve properties throughout the depth of the cloud. The lower MODIS cloud liquid water path can lead to a substantial underestimation of cloud super-cooled liquid water by the CSEA code.

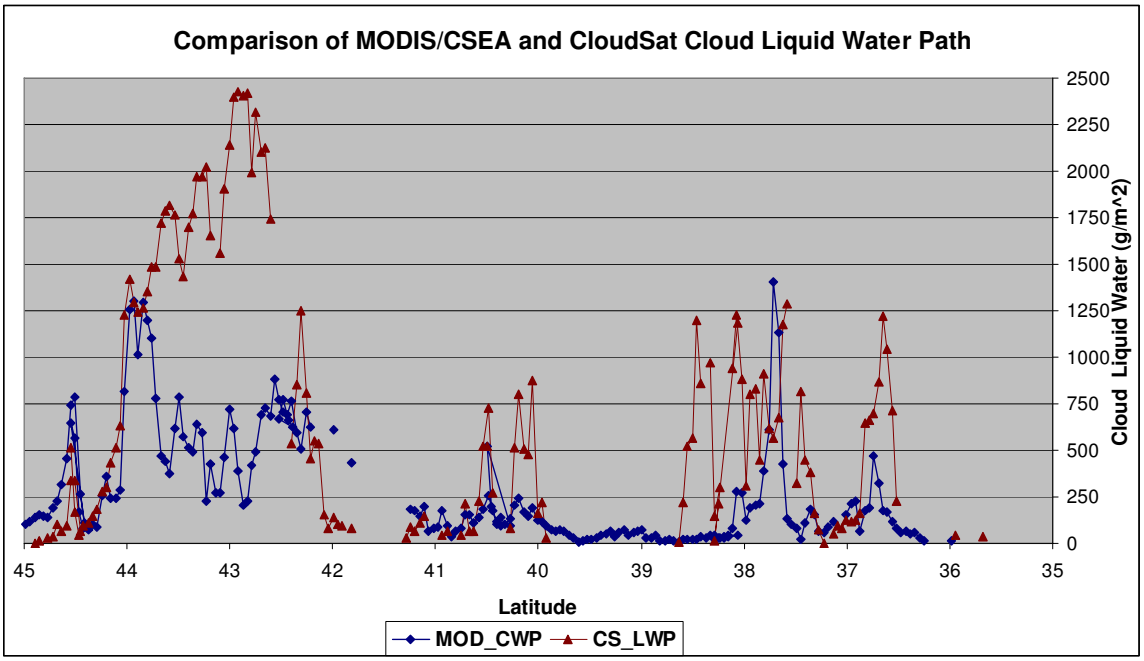

Figure 36. Same as Figure 33 except for cloud liquid water path.

Figure 37 displays the same cloud liquid water path information as Figure 36 but with the product uncertainty values plotted as error bars. The largest uncertainty occurs for clouds with high liquid water concentrations. Although the CloudSat and MODIS values compare better when considering the uncertainty, the differences are still substantial.

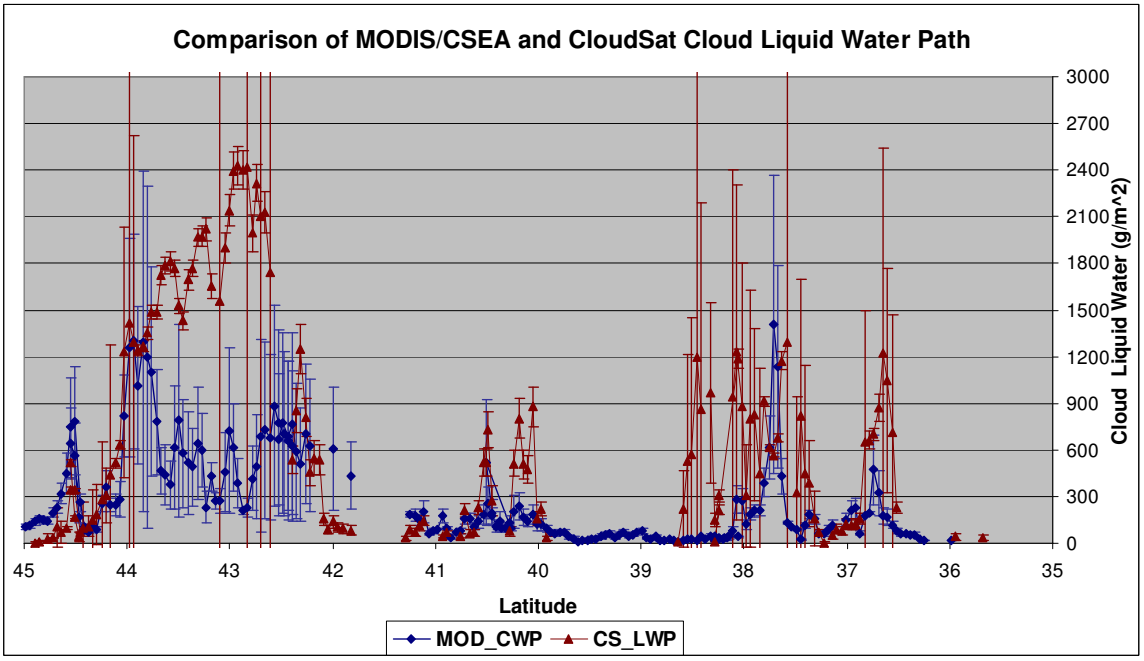

Figure 37. Same as Figure 36 except uncertainty bars are added.

6. SUMMARY AND FUTURE WORK

This report summarizes the work performed at Sandia National Laboratories during the 2009 calendar year for the NMSBA cloud Super-cooled Liquid Water (SLW) project. The major accomplishment during the year was the development of a nearly complete algorithm that is able to produce a spatial estimation of cloud SLW using easily accessible satellite data. This Cloud SLW Estimation Algorithm (CSEA) utilizes MODIS granule level 1 and level 2 data that is collected twice per day during daylight hours from sensors onboard two separate satellite platforms. A minimum of three individual data products must be input to the algorithm that contain geo-location information, derived cloud properties, and the derived cloud mask. Other datasets may be input if clear-sky atmospheric properties are of interest. The algorithm only works for data collected during the daytime since many of the derived products it utilizes are not produced at night. The code can also input certain ground measurements taken at selected locations. A detailed description of the code methodology and structure has been presented. Eighty-one cases from a 14-month period in 2006-2007 were analyzed. These cases were selected due to the existence of sufficient cloud cover over the state of New Mexico. Both spatial data from individual cases and temporal property means have been presented in order to show some of the algorithm results and provide examples of its capability. Sensitivity analysis of many of the program's important parameters were performed and discussed. A preliminary validation of some of the derive properties was made on a single case using derived CloudSat radar cloud products. A procedure was created to accurately compare the CloudSat products with the derived MODIS products as well as some new property estimations from the CSEA code. This single comparison case showed that MODIS data and CSEA products underestimated the four cloud properties examined. The largest difference occurred for derived cloud liquid water. Since this cloud liquid water value forms the basis for the cloud SLW estimation, there exists the potential for underestimating SLW in clouds through the CSEA code.

In the next year, the CSEA code will undergo new enhancements. The primary enhancement will be to develop a GUI that can run the algorithm, produce results, and further assess the derived products. The latter capability would be new and give the user control to perform more detailed analysis of the data and derived products in a given AOI. In addition, the code is to become more concise and streamlined. Input controls will be located in a separate file and there will be new controls on the output. Also, an effort to reduce the manual work required to set-up the input data will be investigated. It may be possible to run the cloud analysis from a single MODIS file, MOD06, since it contains both the geo-location data (at coarser resolution), and a subsection of the 1 km cloud mask. Ambient atmospheric data could be obtained from modeled gridded products instead of ground sites. This spatial model data would require less effort by the user to arrange, be useful anywhere on the globe, and be easier for the algorithm to input and use. It would also provide general atmospheric characteristics at various altitudes across the AOI. Lastly, an automatic procedure to read ground site text files and obtain useful information without manual interaction will be looked into. A user guide will be produced that contains instruction on how to set-up, run, and control the GUI driven software tool.

The validation effort will also continue with more comparisons to spaced-based CloudSat radar derived cloud products and, perhaps, derived cloud properties from ground-based instruments. CloudSat data became available in June 2006. MODIS data from the AQUA satellite and the corresponding CloudSat data will be obtained for longer duration comparisons, including that of an entire day. Further comparisons should provide a better estimate of the MODIS/CSEA derive product bias and global comparisons may uncover regional and/or latitudinal cloud property biases. Validation efforts may be extended to include comparisons of thin cirrus, multilayer cloud, and cloud phase/type. The results of these comparisons may suggest that these cloud properties should play a role in the analysis of cloud SLW. All algorithm methodology changes will be documented in a final report.

APPENDIX. List of the MODIS granule dates.

Table 11. List of the dates and times of the MODIS granules obtained.

Event Number	Year	Date	Time (GMT)	Julian Day
1	2006	11-Mar	1730	70
2	2006	12-Mar	1810	71
3	2006	13-Mar	1715	72
4	2006	15-Mar	1705	74
5	2006	17-Mar	1830	76
6	2006	18-Mar	1735	77
7	2006	22-Mar	1710	81
8	2006	27-Mar	1730	86
9	2006	28-Mar	1810	87
10	2006	1-Apr	1745	91
11	2006	5-Apr	1725	95
12	2006	6-Apr	1805	96
13	2006	10-Apr	1740	100
14	2006	14-Apr	1715	104
15	2006	28-Apr	1730	118
16	2006	5-May	1735	125
17	2006	9-May	1710	129
18	2006	15-May	1810	135
19	2006	22-May	1820	142
20	2006	15-Jun	1730	166
21	2006	5-Jul	1840	186
22	2006	7-Jul	1830	188
23	2006	8-Jul	1735	189
24	2006	27-Jul	1805	208
25	2006	28-Jul	1710	209
26	2006	29-Jul	1755	210
27	2006	30-Jul	1835	211
28	2006	31-Jul	1740	212
29	2006	1-Aug	1825	213
30	2006	3-Aug	1810	215
31	2006	4-Aug	1715	216
32	2006	14-Aug	1755	226
33	2006	15-Aug	1835	227
34	2006	16-Aug	1740	228
35	2006	19-Aug	1810	231
36	2006	20-Aug	1715	232
37	2006	26-Aug	1820	238
38	2006	2-Sep	1825	245
39	2006	3-Sep	1730	246
40	2006	4-Sep	1810	247
41	2006	7-Sep	1705	250
42	2006	8-Sep	1745	251
43	2006	22-Sep	1800	265
44	2006	6-Oct	1810	279
45	2006	8-Oct	1800	281

Event Number	Year	Date	Time (GMT)	Julian Day
46	2006	9-Oct	1705	282
47	2006	24-Oct	1800	297
48	2006	13-Nov	1735	317
49	2006	29-Nov	1735	333
50	2006	19-Dec	1710	353
51	2006	30-Dec	1830	364
52	2007	5-Jan	1755	5
53	2007	12-Jan	1800	12
54	2007	19-Jan	1805	19
55	2007	20-Jan	1710	20
56	2007	22-Jan	1835	22
57	2007	23-Jan	1740	23
58	2007	30-Jan	1750	30
59	2007	1-Feb	1735	32
60	2007	11-Feb	1810	42
61	2007	13-Feb	1800	44
62	2007	8-Mar	1805	67
63	2007	10-Mar	1755	69
64	2007	11-Mar	1835	70
65	2007	12-Mar	1740	71
66	2007	22-Mar	1820	81
67	2007	23-Mar	1725	82
68	2007	24-Mar	1805	83
69	2007	30-Mar	1730	89
70	2007	6-Apr	1735	96
71	2007	7-Apr	1820	97
72	2007	8-Apr	1725	98
73	2007	9-Apr	1805	99
74	2007	12-Apr	1835	102
75	2007	13-Apr	1740	103
76	2007	21-Apr	1830	111
77	2007	24-Apr	1725	114
78	2007	2-May	1810	122
79	2007	5-May	1705	125
80	2007	6-May	1750	126
81	2007	8-May	1735	128

REFERENCES

Chakrapani, V., D. R. Doelling, A. D. Rapp, and P. Minnis, 2002: Cloud thickness estimation from GOES-8 satellite data over the ARM SGP site. In *Proceedings of the Twelfth Atmospheric Radiation Measurement (ARM) Science Team Meeting*, ARM-CONF-2002.

Doutriaux-Boucher, M., and J. Quaas, 2004: Evaluation of cloud thermodynamic phase parametrizations in the LMDZ GCM by using POLDER satellite data, *Geophys. Res. Lett.*, 31, L06126, doi:10.1029/2003GL019095.

Menzel, W. P., R. A. Frey, B. A. Baum, H. Zhang, 2004: Cloud Top Properties And Cloud Phase Algorithm Theoretical Basis Document, (atbd_mod04), available at: http://modis.gsfc.nasa.gov/data/atbd/atmos_atbd.php.

Minnis, P., W. L. Smith, Jr., D. P. Garber, J. K. Ayers, and D. R. Doelling, 1995: "Cloud properties derived from GOES-7 for Spring 1984 ARM Intensive Observing Period using Version 1.0.0 of ARM satellite data analysis program," NASA RP 1366, p.58.

Roskovensky, J., M. Ivey, and N. Beavis, SAND Report (2009-1133), 2009: New Mexico Cloud Super-Cooled Liquid Water Survey, Final Report 2008.

DISTRIBUTION

Electronic Distribution

MS0406	Toby Townsend	05713
MS0406	John Roskovensky	05713
MS0734	Joe Tillerson	06338
MS0734	Bernard Zak	06338
MS0734	Mark Ivey	06338
MS0899	Technical Library	04536